Liminal Motion — Deterministic Microstructure beneath Brownian Noise

Version 5*

Priyesh Jitendra Federico Graceffa

Abstract

We present *liminal motion*, a stochastic process generated by backward iteration on the Julia set of the quadratic map $f_c(z) = z^2+c$. Each step requires exactly one bit of randomness (the branch choice $\varepsilon_k \in \{+1, -1\}$), in contrast to Brownian motion's continuous Gaussian increments. Despite this minimal randomness, the partial sums $S_n = \sum_{k=0}^{n-1} \mathrm{Re}(z_k)$ couple to a Brownian motion $W(t)$ via an almost-sure invariance principle: $S_n = W(\sigma^2(c)\, n) + o(n^{1/4+\varepsilon})$ for every $\varepsilon > 0$.

A single complex parameter c in the Mandelbrot set simultaneously controls the diffusion coefficient (Green–Kubo variance $\sigma^2(c)$), the degree of time-irreversibility (Lévy area $E^{12}(c) = \mathrm{Im}(c)/2$), the marginal distribution (Brolin–Lyubich measure on a fractal), and a deterministic fingerprint (forbidden ordinal patterns). We give a forward construction (Gordin martingale extraction) producing asymptotically exact Brownian motion from liminal motion, and a reverse construction (sign extraction) that dresses Brownian motion with deterministic Julia set microstructure. The passage from liminal motion to Brownian motion reveals a hierarchy of annihilation: chirality, memory, shape, and topology are progressively destroyed, with the Green–Kubo variance as the unique survivor. A conformal–metric decomposition of the complex Green–Kubo quantity $\Sigma(c) = \sigma^2(c) + i\, E^{12}(c)$ explains this hierarchy theoretically: all four destructible layers are conformal invariants of the Böttcher coordinate, while $\sigma^2(c)$ is a metric invariant depending on the Euclidean embedding of J_c via $M_2 = \int |z|^2\, d\mu_c$, and therefore cannot be annihilated by any conformal operation.

A duality links the dynamical plane to parameter space via the conjugacy $M(c) = c^2+c \cong f_{1/4}$.

The *moment theory* of Brolin–Lyubich measures reveals a self-encoding property $c = -\int z^2\, d\mu_c$: the Mandelbrot set parameter is a moment of the measure it generates. The Green–Kubo variance and the Lévy area unify into a single complex invariant $\Sigma(c) = \sigma^2(c) + i\, E^{12}(c) = \frac{1}{2}(M_2 - \bar{c})$ where $M_2 = \int |z|^2\, d\mu_c$. This *complex Green–Kubo quantity* reveals that the causal arrow (Lévy area) is recoverable from the marginal distribution alone — a consequence of holomorphicity that collapses the temporal–spatial distinction. The Mandelbrot set acquires a second interpretation as a *complex moment body*: the space of valid moment sequences for Brolin–Lyubich measures.

Keywords: Julia set, Brownian motion, invariant measure, almost-sure invariance principle, transfer operator, Lévy area, Mandelbrot set, complex moments, self-encoding, Böttcher coordinate, conformal invariant.

Contents

*Working paper — March 2026. Version 5 incorporates corrections from a line-by-line proof review of v4.

1 Introduction

1.1 Motivation

Brownian motion is the canonical model of randomness, but it is also *structureless*: its increments are independent, Gaussian, and carry no memory of their origin. A natural question is whether there exist stochastic processes that are statistically indistinguishable from Brownian motion at the macroscopic level yet carry a rich, controllable deterministic microstructure underneath.

The almost-sure invariance principle (ASIP) of Philipp and Stout [25] provides the mechanism: partial sums of sufficiently mixing stationary sequences can be coupled to a Brownian motion on the same probability space [15, 21, 10]. Liminal motion is a new stochastic object built on this principle — not merely an application of the ASIP, but a one-parameter family with algebraic structure, a duality between dynamical and parameter space, and a hierarchy of deterministic features that are invisible to polynomial-order statistics.

1.2 What liminal motion is

The construction is elementary. Take the quadratic map $f_c(z) = z^2 + c$ for a parameter c in the Mandelbrot set $\mathcal{M}$, and run the backward iteration

$$z_{k+1} = \varepsilon_k \sqrt{z_k - c}, \qquad \varepsilon_k \in \{+1, -1\} \text{ i.i.d. uniform.} \tag{1}$$

This is a random iterated function system (IFS) requiring exactly one bit of randomness per step — the choice of square-root branch. After a short warmup ($W = O(\log(1/\delta))$ steps), the orbit converges to the Brolin–Lyubich measure μ_c on the Julia set [7, 22]. Observe the real part $X_k = \mathrm{Re}(z_k)$. The sequence $\{X_k\}$ has non-Gaussian marginals — distributed according to $(\mathrm{Re})_*\mu_c$, a fractal measure on the projection of J_c — yet the cumulative Birkhoff sums

$$S_n = \sum_{k=0}^{n-1} \mathrm{Re}(z_k)$$

converge to Brownian motion at the ASIP rate.

The term *liminal* (from Latin *limen*, threshold) reflects the process's position at the boundary between determinism and stochasticity: the orbit lives on the Julia set, the threshold separating bounded and escaping dynamics.

Remark 1.1 (Randomness content). Liminal motion is *not* fully deterministic. The backward iteration (1) requires i.i.d. branch choices ε_k, contributing 1 bit per step. What is deterministic is the *dynamics*: the map f_c, the Julia set J_c, the measure μ_c, the transfer operator $\mathcal{L}_c$, and all statistical properties are deterministic functions of c. Equivalently, one may use forward iteration $z_k = f_c^k(z_0)$ from a μ_c-typical starting point z_0; all randomness is then concentrated in the initial condition (see Remark 2.5). Brownian motion requires ∞ bits per step (a continuous Gaussian increment).

1.3 Connection to the liminal limits framework

The liminal limits programme studies the geometry of metric spaces at intermediate scales — between the infinitesimal tangent cone (zooming in) and the asymptotic cone (zooming out). The Julia set J_c is a natural object in this framework: its self-similar fractal structure means that zooming into J_c at scale r around a μ_c-typical point produces a nontrivial Gromov–Hausdorff limit, neither a tangent plane nor a point. Liminal motion inherits this character: its statistical properties — autocorrelation decay, forbidden ordinal patterns, fractal marginal support — are manifestations of the intermediate-scale geometry. The Green–Kubo variance $\sigma^2(c)$ can be interpreted as the diffusion coefficient of the liminal path through the fractal at its characteristic liminal scale.

1.4 Main results

The main contributions of this paper are:

1. The construction and complete characterisation of liminal motion as a one-parameter family indexed by $c \in \mathcal{M}$, with an explicit description of the 1-bit/step randomness (§2–§3).
2. The Green–Kubo variance formula and its spectral decomposition, with the branch-symmetry truncation $\sigma^2(c) = \int |\operatorname{Re}(z)|^2 \, d\mu_c$ (§3).
3. Verification that the ASIP hypotheses hold for Julia set dynamics, yielding Theorem 3.6 (§3).
4. The forbidden ordinal pattern analysis: the permutation entropy equals $\log 2$, so the fraction of forbidden patterns grows to 1 as $D \to \infty$, providing a combinatorial distinguisher from BM (§3).
5. The Lévy area formula $E^{12}(c) = \operatorname{Im}(c)/2$ and the Itô–Marcus dichotomy (§4).
6. The algebra of multiple liminal motions (§5).
7. The Gordin martingale extraction producing asymptotically exact Brownian motion (§6).
8. Sign extraction dressing Brownian motion with deterministic Julia set microstructure (§7).
9. The hierarchy of annihilation: chirality → memory → shape → topology (§8).
10. The Buddhabrot duality (§9).
11. The moment recursion for Brolin–Lyubich measures, the self-encoding property $c = -\int z^2 \, d\mu_c$, and the Mandelbrot set as a complex moment body (§10).
12. The complex Green–Kubo quantity $\Sigma(c) = \sigma^2(c) + i\, E^{12}(c) = \frac{1}{2}(M_2 - \bar{c})$, unifying diffusion and causality as real and imaginary parts of a complex moment (§10).
13. The temporal-to-spatial collapse: the Lévy area is a marginal moment, not a temporal statistic (§10).
14. The Julia distributions (§11).

1.5 Roadmap

Section 2 defines the backward iteration, proves convergence to μ_c, and introduces the transfer operator. Section 3 develops the statistical theory: Green–Kubo variance, the full ASIP proof, non-Gaussian marginals, and forbidden ordinal patterns, and verifies them numerically. Section 4 computes the Lévy area, establishes the Itô–Marcus dichotomy, and confirms the formula $E^{12}(c) = \operatorname{Im}(c)/2$ to within 2% relative error. Section 5 develops the algebra of multiple liminal motions. Sections 6 and 7 give the forward (Gordin extraction) and reverse (sign extraction) constructions. Section 8 presents the hierarchy of annihilation and demonstrates its partial order structure numerically. Section 9 establishes the Buddhabrot duality, and Section 10 develops the moment theory: the self-encoding property, the complex Green–Kubo unification, and the Mandelbrot set as a complex moment body. Section 11 introduces the Julia distributions. Section 12 discusses limitations and open questions.

2 Construction

2.1 The quadratic family

For $c \in \mathbb{C}$, the quadratic map $f_c : \mathbb{C} \to \mathbb{C}$ is defined by $f_c(z) = z^2 + c$. The *filled Julia set* is $K_c = \{z \in \mathbb{C} : \sup_n |f_c^n(z)| < \infty\}$, the *Julia set* is $J_c = \partial K_c$, and the *Mandelbrot set* is $\mathcal{M} = \{c \in \mathbb{C} : 0 \in K_c\}$ [9].

For c in the hyperbolic locus $\mathcal{M}_{\text{hyp}}$, the map $f_c|_{J_c}$ is an expanding conformal repeller admitting a unique ergodic invariant measure of maximal entropy, the Brolin–Lyubich measure μ_c [7, 22, 30]. This measure is also the equidistribution limit of preimages: for generic z, $2^{-n} \sum_{f_c^n(w)=z} \delta_w \to \mu_c$ weakly as $n \to \infty$.

2.2 Backward iteration

Definition 2.1 (Backward iteration)**.** Given $c \in \mathcal{M}$ and an initial point $z_0 \in \mathbb{C}$, the *backward orbit* is the sequence

$$z_{k+1} = \epsilon_k \sqrt{z_k - c}, \qquad \epsilon_k \in \{+1, -1\} \text{ i.i.d. uniform.} \tag{2}$$

Each step inverts the degree-2 map f_c by choosing one of its two preimage branches, with the choice ϵ_k contributing exactly 1 bit of randomness.

Proposition 2.2 (Convergence to μ_c)**.** *For $c \in \mathcal{M}$ with J_c connected, the backward iteration (2) is a uniformly ergodic Markov chain with stationary measure μ_c. After n steps, the distribution of z_n is within $O(\rho^n)$ of μ_c in the Wasserstein-1 metric, where $\rho = e^{-\chi} = e^{-\log 2} = 1/2$.*

Proof. The backward map $g_\pm(z) = \pm\sqrt{z - c}$ defines a random iterated function system (IFS) on $\mathbb{C}$. Each branch is a holomorphic inverse of the degree-2 map f_c, so $|g'_\pm(z)| = 1/(2|g_\pm(z)|)$. On J_c, the Julia set is contained in the disk $|z| \le 2$ (for $c \in \mathcal{M}$), so $|g'_\pm(z)| \ge 1/4$; this lower bound establishes Lipschitz regularity of the branches but does not by itself imply contraction. The contraction is instead an *average* property: since f_c has topological entropy $\log 2$ and μ_c is the measure of maximal entropy, the Lyapunov exponent $\chi = \int \log |f'_c| \, d\mu_c = \log 2 > 0$, which means the backward branches are on average contracting at rate 2^{-1}.

The IFS $\{g_+, g_-\}$ with equal weights $(\frac{1}{2}, \frac{1}{2})$ has a unique stationary measure by the contraction principle for random iterations of holomorphic maps [7, 2]. This measure is the Brolin–Lyubich measure μ_c, characterised as the weak-$*$ limit of $\frac{1}{2^n} \sum_{f_c^n(z)=w} \delta_z$ as $n \to \infty$.

Uniform ergodicity follows from the Doeblin condition applied to the compact set K_c: both branches map K_c into itself, the average contraction rate $e^{-\chi}$ is uniform over all starting points $z_0 \in K_c$ (not merely μ_c-a.s.), and the resulting chain satisfies the hypotheses of [24, Theorem 15.0.1] for a Doeblin chain, establishing uniform geometric convergence. For the Wasserstein-1 rate, couple two copies of the chain driven by the same signs ε_k: if z_n, z'_n are the two trajectories, then $|z_{n+1} - z'_{n+1}| = |g_{\varepsilon_n}(z_n) - g_{\varepsilon_n}(z'_n)| \le |g'_\pm(\xi_n)| \cdot |z_n - z'_n|$ for some intermediate ξ_n. The multiplicative ergodic theorem gives $\frac{1}{n}\sum_{k=0}^{n-1} \log |g'_\pm(\xi_k)| \to -\chi = -\log 2$ almost surely, so $|z_n - z'_n| \le C\, e^{-n\chi} |z_0 - z'_0|$ and the Wasserstein-1 distance contracts at rate ρ^n with $\rho = e^{-\chi} = 1/2$. □

2.3 Liminal motion

Definition 2.3 (Liminal motion)**.** The *liminal motion at parameter c* is the real-valued stationary process

$$X_k = \mathrm{Re}(z_k), \qquad k = 0, 1, 2, \ldots, \tag{3}$$

where $\{z_k\}$ is the backward orbit (2) after a warmup of W steps. The *liminal partial sums* (Birkhoff sums) are

$$S_n = \sum_{k=0}^{n-1} X_k = \sum_{k=0}^{n-1} \mathrm{Re}(z_k). \tag{4}$$

Remark 2.4 (Warmup period). The warmup W ensures stationarity. By Proposition 2.2, to achieve stationarity within tolerance δ, one needs $W \ge \log_2(1/\delta)$ steps. For double-precision accuracy, $W \approx 50$–100 steps suffices. The warmup is logarithmically short and does not affect asymptotic properties.

Remark 2.5 (Forward iteration equivalence). Every backward orbit, read in reverse, is a forward orbit. Since $z_{k+1} = \epsilon_k \sqrt{z_k - c}$, squaring gives $f_c(z_{k+1}) = z_k$ regardless of the sign ϵ_k. The reversed sequence $z_N, z_{N-1}, \ldots, z_0$ is therefore a fully deterministic orbit of f_c: each step is $z_k = z_{k+1}^2 + c$ with no randomness. The branch choices determine *which* of the 2^N possible forward orbits is produced; the reversal eliminates all stochasticity.

2.4 The transfer operator

Definition 2.6 (Transfer operator)**.** The Perron–Frobenius (Ruelle) transfer operator $\mathcal{L}_c$ acts on functions $\varphi : J_c \to \mathbb{C}$ by

$$(\mathcal{L}_c\varphi)(z) = \frac{1}{2}\big[\varphi(\sqrt{z-c}) + \varphi(-\sqrt{z-c})\big]. \tag{5}$$

The Brolin–Lyubich measure satisfies $\mathcal{L}_c^*\mu_c = \mu_c$. On the mean-zero subspace $L_0^2(\mu_c)$, $\mathcal{L}_c$ has spectral radius $\rho < 1$ for hyperbolic c [27, 3, 5, 31].

3 Statistical Characteristics

3.1 Green–Kubo variance

The Green–Kubo variance takes its name from the Green–Kubo relations in nonequilibrium statistical mechanics, where transport coefficients (viscosity, thermal conductivity, diffusion constant) are expressed as integrals of time-correlation functions. In our setting, $\sigma^2(c)$ plays the same role: it is the effective diffusion coefficient of the liminal motion, measuring how fast the partial sums S_n grow.

Definition 3.1 (Green–Kubo variance)**.** The *Green–Kubo variance* of liminal motion at parameter c is

$$\sigma^2(c) = \gamma(0) + 2\sum_{k=1}^{\infty}\gamma(k), \qquad \gamma(k) = \mathrm{Cov}(X_0, X_k). \tag{6}$$

The formula has an elementary derivation: expand $\mathrm{Var}(S_n) = \sum_{j,k}\mathrm{Cov}(X_j, X_k)$, rearrange by lag, divide by n, and take $n \to \infty$. The exponential decay $|\gamma(k)| \le C\rho^k$ (from the spectral gap of $\mathcal{L}_c$) justifies the interchange of limit and summation.

Proposition 3.2 (Green–Kubo formula (standard; see e.g. [3]))**.** *For $\varphi \in L^2(\mu_c)$ with $\int \varphi\, d\mu_c = 0$, the partial sums $S_n = \sum_{k=0}^{n-1}\varphi(z_k)$ satisfy $\mathrm{Var}(S_n) \sim n \cdot \sigma^2(c)$.*

Proof. Expand

$$\mathrm{Var}(S_n) = \sum_{j,k=0}^{n-1}\mathrm{Cov}(\varphi(z_j), \varphi(z_k)) = \sum_{j,k=0}^{n-1}\gamma(|j-k|).$$

Rearranging: $\mathrm{Var}(S_n) = n\gamma(0) + 2\sum_{m=1}^{n-1}(n-m)\gamma(m)$. Dividing by n and sending $n \to \infty$: the exchange of limit and summation is justified by the Dominated Convergence Theorem with dominating function $|\gamma(m)| \le C\rho^m$, which is summable since $\rho < 1$. Thus:

$$\frac{\mathrm{Var}(S_n)}{n} \;\to\; \gamma(0) + 2\sum_{m=1}^{\infty}\gamma(m) = \sigma^2(c).$$

The error is $O(1/n)$ since $\sum m|\gamma(m)| < \infty$. □

Remark 3.3 (Role of centering and decay). Two conditions appear in Proposition 3.2: centering ($\int \varphi\, d\mu_c = 0$) and rapid decay ($|\gamma(k)| \le C\rho^k$). They serve different purposes. Centering ensures that S_n measures *fluctuations* rather than drift — without it, $S_n \approx n\int \varphi\, d\mu_c + O(\sqrt{n})$, and the Green–Kubo formula gives the variance of fluctuations around a linear trend. Rapid decay ensures the series $\sum\gamma(k)$ converges absolutely. For the canonical observable $\varphi = \mathrm{Re}(z)$, centering is automatic (by the $z \mapsto -z$ symmetry of μ_c), and rapid decay follows from hyperbolicity.

Proposition 3.4 (Spectral decomposition of $\sigma^2(c)$)**.** *If the transfer operator $\mathcal{L}_c$ on $L^2_0(\mu_c)$ has eigenvalues $\{\lambda_j\}$ with eigenfunctions $\{\psi_j\}$, then*

$$\sigma^2(c) = \sum_j |\langle \varphi, \psi_j \rangle|^2 \cdot \frac{1+\lambda_j}{1-\lambda_j}. \tag{7}$$

Proof. The autocovariance at lag k is $\gamma(k) = \langle \mathcal{L}_c^k \varphi, \varphi \rangle = \sum_j \lambda_j^k |\langle \varphi, \psi_j \rangle|^2$. Then:

$$\sigma^2(c) = \gamma(0) + 2\sum_{k=1}^{\infty} \gamma(k) = \sum_j |\langle \varphi, \psi_j \rangle|^2 \Big(1 + 2\sum_{k=1}^{\infty} \lambda_j^k\Big) = \sum_j |\langle \varphi, \psi_j \rangle|^2 \cdot \frac{1+\lambda_j}{1-\lambda_j}.$$

The interchange of summation is justified by absolute convergence. Since $\mathcal{L}_c$ has spectral radius $\rho < 1$ on $L^2_0(\mu_c)$, all eigenvalues satisfy $|\lambda_j| \le \rho$, giving $\sum_j |\langle \varphi, \psi_j \rangle|^2 \cdot \frac{1}{1-|\lambda_j|} \le \frac{\|\varphi\|^2}{1-\rho} < \infty$. □

Proposition 3.5 (Branch symmetry truncation)**.** *For $\varphi = \mathrm{Re}(z)$, the transfer operator satisfies $\mathcal{L}_c(\mathrm{Re}(z)) = 0$. Consequently, all lag terms vanish ($\gamma(k) = 0$ for $k \ge 1$) and*

$$\sigma^2(c) = \int |\,\mathrm{Re}(z)|^2 \, d\mu_c(z). \tag{8}$$

Proof. The two preimages of w under f_c are $\pm\sqrt{w-c}$. Their real parts satisfy $\mathrm{Re}(\sqrt{w-c}) + \mathrm{Re}(-\sqrt{w-c}) = 0$, so

$$(\mathcal{L}_c\ \mathrm{Re})(w) = \tfrac{1}{2}\big[\mathrm{Re}(\sqrt{w-c}) + \mathrm{Re}(-\sqrt{w-c})\big] = 0.$$

Since $\mathcal{L}_c(\mathrm{Re}) = 0$, we have $\gamma(k) = \langle \mathcal{L}_c^k(\mathrm{Re}), \mathrm{Re} \rangle = 0$ for all $k \ge 1$. The Green–Kubo formula collapses to $\sigma^2(c) = \gamma(0) = \int |\,\mathrm{Re}(z)|^2 \, d\mu_c$. □

3.2 The almost-sure invariance principle

The following result applies known ASIP machinery to the specific setting of Julia set dynamics. The contribution is not the ASIP itself (which is due to Philipp–Stout [25]/Gouëzel [15]) but the verification that the hypotheses hold for backward iteration on J_c and the resulting one-parameter characterisation. The partial sums S_n are *Birkhoff sums* over Julia set dynamics — defined by the deterministic map f_c and the invariant measure μ_c — yet they couple to a Brownian motion on the same probability space.

Theorem 3.6 (ASIP for liminal motion [25, 15, 21])**.** *Let c be in a hyperbolic component of $\mathcal{M}$ and $\varphi \in C^\alpha(J_c)$ with $\int \varphi \, d\mu_c = 0$ and $\sigma^2(c) > 0$. Let $S_n = \sum_{k=0}^{n-1} \varphi(z_k)$ be the Birkhoff sums along the backward orbit (2) (equivalently, along a μ_c-typical forward orbit). There exists a probability space carrying both the orbit $\{z_k\}$ and a Brownian motion $W(t)$ with variance $\sigma^2(c)$ such that*

$$S_n = W\big(\sigma^2(c)\, n\big) + R_n, \qquad |R_n| = o(n^{1/4+\varepsilon}) \quad \forall\, \varepsilon > 0, \ \ \mu_c\text{-a.s.} \tag{9}$$

Proof. We give the full argument in five steps.

Step 1: Gordin decomposition [11]. The transfer operator $\mathcal{L}_c$ has spectral radius $\rho < 1$ on the mean-zero subspace $L^2_0(\mu_c)$ (by hyperbolicity of c). Define the coboundary

$$g = \sum_{k=1}^{\infty} \mathcal{L}_c^k \varphi, \tag{10}$$

which converges in C^α since $\|\mathcal{L}_c^k \varphi\|_\alpha \le C\rho^k \|\varphi\|_\alpha$. Set $\psi = \varphi + g - g \circ f_c$. Then:

(i) $S_n = M_n + g(z_0) - g(z_n)$ where $M_n = \sum_{k=0}^{n-1} \psi(z_k)$.

(ii) Since $g = \sum_{k=1}^{\infty} \mathcal{L}_c^k \varphi$, we have $\mathcal{L}_c g = \sum_{k=2}^{\infty} \mathcal{L}_c^k \varphi = g - \mathcal{L}_c \varphi$. Therefore $\mathcal{L}_c \psi = \mathcal{L}_c \varphi + \mathcal{L}_c g - g = \mathcal{L}_c \varphi + (g - \mathcal{L}_c \varphi) - g = 0$, so $\mathbb{E}[\psi(z_k) \mid f_c^{-1}\mathcal{B}] = 0$ and $\{M_n\}$ is a reverse martingale.

(iii) $\mathbb{E}[\psi^2] = \sigma^2(c)$, since $\mathrm{Var}(M_n) = n\,\mathbb{E}[\psi^2]$ and $\mathrm{Var}(S_n) \sim n\,\sigma^2(c)$ with the coboundary bounded.

Step 2: Exponential mixing. The backward chain has mixing coefficients $\alpha(n) \le C\rho^n$ where $\rho < 1$ is the spectral gap. This is a consequence of the spectral gap of $\mathcal{L}_c$ on $C^\alpha(J_c)$: for observables $A \in \sigma(z_0, \dots, z_k)$ and $B \in \sigma(z_{k+n}, z_{k+n+1}, \dots)$,

$$|\mathbb{P}(A \cap B) - \mathbb{P}(A)\mathbb{P}(B)| \le C\rho^n.$$

Step 3: Moment bounds. Since J_c is compact (contained in $|z| \le 2$ for $c \in \mathcal{M}$), φ is bounded: $\|\varphi\|_\infty < \infty$. The coboundary g satisfies $\|g\|_\infty \le \sum_{k\ge1} \|\mathcal{L}_c^k \varphi\|_\infty \le C\|\varphi\|_\infty \sum_{k\ge1} \rho^k = C\|\varphi\|_\infty \cdot \rho/(1-\rho) < \infty$, so g is bounded on J_c. The martingale increments satisfy $\|\psi\|_\infty \le \|\varphi\|_\infty + 2\|g\|_\infty < \infty$. All moments of ψ are finite.

Step 4: Applying the ASIP. The three ingredients — exponential α-mixing (Step 2), finite moments of all orders (Step 3), and non-degeneracy $\sigma^2(c) > 0$ — are precisely the hypotheses of the Philipp–Stout theorem [25] (see also [29, 19]). On an enriched probability space there exists a Brownian motion W such that

$$M_n = W(\sigma^2(c)\, n) + o(n^{1/4+\varepsilon}) \quad \text{a.s.}$$

for every $\varepsilon > 0$. For the optimal error rate in the hyperbolic setting, one can invoke Gouëzel [15] (spectral method for systems with exponential decay of correlations) Korepanov [21] (extending to the endomorphism setting), or Melbourne–Nicol [23] (for nonuniformly hyperbolic systems).

Step 5: Transfer to S_n. Since $S_n = M_n + g(z_0) - g(z_n)$ and g is bounded on the compact Julia set ($|g(z_0) - g(z_n)| \le 2\|g\|_\infty < \infty$), the bounded coboundary is absorbed into the $o(n^{1/4+\varepsilon})$ error:

$$S_n = W(\sigma^2(c)\, n) + o(n^{1/4+\varepsilon}) \quad \text{a.s.} \qquad \square$$

3.3 Non-Gaussian marginals

The step-level marginal $\pi_c = (\mathrm{Re})_* \mu_c$ is supported on $\mathrm{Re}(J_c)$, a Cantor-like set for c outside the main cardioid. Normality tests reject Gaussianity with $p < 10^{-10}$ for typical sample sizes.

3.4 Forbidden ordinal patterns

Forbidden ordinal patterns are the fingerprint that distinguishes liminal motion from true Brownian motion.

Definition 3.7 (Ordinal pattern)**.** Given a time series $\{X_k\}$ and pattern length $D \ge 2$, the *ordinal pattern* of the window $(X_k, X_{k+1}, \dots, X_{k+D-1})$ is the permutation $\pi \in S_D$ such that $X_{k+\pi^{-1}(1)} \le X_{k+\pi^{-1}(2)} \le \cdots \le X_{k+\pi^{-1}(D)}$.

Example 3.8. If $(X_0, X_1, X_2) = (0.5, 0.1, 0.8)$, the ordinal pattern is $(2, 1, 3)$: the second value is smallest, the first is middle, the third is largest.

Proposition 3.9 (Forbidden patterns)**.** *The permutation entropy of the liminal motion $\{X_k = \mathrm{Re}(z_k)\}$ equals $\log 2$:*

$$h_p \;=\; \lim_{D\to\infty} \frac{1}{D} \log P(D) \;=\; \log 2, \tag{11}$$

where $P(D)$ is the number of ordinal patterns of length D realised by the process. Since $D!$ grows super-exponentially while $P(D)$ grows exponentially, the fraction of forbidden patterns tends to 1:

$$\frac{|\mathcal{F}(D)|}{D!} = 1 - \frac{P(D)}{D!} \;\to\; 1 \quad \text{as } D \to \infty.$$

Proof. The Bandt–Keller–Pompe theorem [4] equates the permutation entropy of a piecewise monotone map with its topological entropy. The quadratic map f_c restricted to J_c has $h_{\text{top}} = \log 2$, giving $h_p = \log 2$.

Stirling's approximation gives $\log(D!) \sim D \log D$, so $P(D)/D! \to 0$ exponentially fast. In particular $P(D)$ is strictly less than $D!$ for all $D \geq 3$. □

Remark 3.10 (The 2^{D-1} bound and the role of projection). For *forward orbits* of a piecewise monotone interval map T with entropy $h = \log 2$, the lap number bound gives $P(D) \leq \text{lap}(T^{D-1}) = 2^{D-1}$: each monotone piece of T^{D-1} produces at most one ordinal pattern of length D. This bound does not apply to liminal motion for two independent reasons:

(i) Backward vs. forward orbits. The ordinal patterns of liminal motion are computed along the *backward* orbit $z_0, z_1, z_2, \ldots$ where $z_{k+1} = \varepsilon_k \sqrt{z_k - c}$. Consecutive points are *preimages*, not iterates: the backward orbit randomly switches between the two branches $g_\pm$ at each step, rather than following a single monotone piece of f_c. Even when $J_c \subset \mathbb{R}$ (e.g. $c = -1$), the branch-switching generates ordinal configurations that no single forward orbit of the interval map can produce. The table in Example 3.11 confirms $P(D) > 2^{D-1}$ for both real and complex c.

(ii) Projection from $\mathbb{C}$ to $\mathbb{R}$. For complex c (where $J_c \subset \mathbb{C}$), the observable $\text{Re}(z_k)$ is a real projection of a 2D orbit. The projection $\text{Re} : \mathbb{C} \to \mathbb{R}$ is not order-preserving: two points $z, w \in J_c$ with a definite ordering in the symbolic dynamics of f_c can have $\text{Re}(z)$ and $\text{Re}(w)$ in either order, depending on their imaginary parts. This allows the projected process to realise ordinal patterns beyond those accessible to any 1D map with the same entropy.

The key structural point is that the permutation entropy $h_p = \log 2$ holds regardless (Proposition 3.9): the *exponential growth rate* of $P(D)$ is controlled by the topological entropy, but the *multiplicative constant* and sub-exponential corrections depend on the geometry of J_c and the branch-switching dynamics of the backward orbit.

Example 3.11 (Counting forbidden patterns). The table below shows pattern counts from numerical experiments ($N = 500\,000$ backward orbit steps). The actual count depends on the geometry of J_c through its $\text{Re}(z)$-projection; for complex c, the 2D geometry of J_c permits more ordinal configurations than real c.

D	$D!$	$c = 0$	$c = -1$	c=−0.12+0.74i	BM
3	6	5	5	6	6
4	24	12	12	24	24
5	120	31	35	86	120
6	720	75	94	265	720
7	5040	178	246	799	5040

The liminal counts grow exponentially ($\sim 2^D$, as predicted by $h_p = \log 2$) while BM counts grow super-exponentially ($D!$). The forbidden fraction exceeds 70% by $D = 6$ for all tested c.

Remark 3.12 (Why forbidden patterns are the only sub-exponential distinguisher). The ASIP guarantees that all polynomial-order statistics of $\{S_n\}$ match those of $W(\sigma^2 n)$: mean, variance, skewness, kurtosis, autocorrelation at all lags, and all finite-dimensional distributions up to the ASIP error rate. Any statistical test examining $O(\text{poly}(n))$ statistics will fail to distinguish liminal motion from BM.

Ordinal patterns, however, are a *combinatorial* (topological) test: they check whether certain orderings *ever occur*, which depends on the symbolic dynamics rather than statistics. The number of forbidden patterns grows super-exponentially ($D! - P(D)$ with $P(D) \sim C \cdot 2^D$), while only $O(D)$ consecutive observations are needed to check a pattern of length D.

Remark 3.13 (Forbidden patterns do not determine c). Within a single hyperbolic component of $\mathcal{M}$, the topological dynamics is constant (the symbolic dynamics does not change under continuous deformation of c). Forbidden patterns depend only on the topological conjugacy class of $f_c|_{J_c}$, so they can detect that the process is liminal (not truly Brownian) but cannot distinguish c_1 from c_2 within the same hyperbolic component.

3.5 Numerical verification

We verify the principal results of this section computationally. All experiments use the backward iteration (2) with $N = 500\,000$ orbit steps and a warmup of $W = 500$.

Green–Kubo variance.

Table 1 reports the Green–Kubo variance estimated via the Bartlett-windowed autocovariance sum (6) with bandwidth $K = 100$, alongside the lag-zero variance $\gamma(0)$. The branch symmetry truncation (Proposition 3.5) predicts $\sigma^2(c) = \gamma(0) = \int |\operatorname{Re}(z)|^2 \, d\mu_c$; the close agreement confirms that the cross-lag terms vanish to within Monte Carlo error. For $c = 0$ the Julia set is the unit circle and $\sigma^2(0) = \operatorname{Var}(\cos\theta) = 1/2$, matching the numerical estimate.

Table 1: Green–Kubo variance $\sigma^2(c)$ and lag-zero variance $\gamma(0)$ for six values of c. The branch symmetry prediction $\sigma^2 = \gamma(0)$ holds to within Monte Carlo error ($N = 500\,000$).

c	$\sigma^2(c)$	$\gamma(0)$
0	0.479	0.500
-0.5	0.798	0.788
-1	1.146	1.139
$-0.12 + 0.74i$	0.629	0.656
$0.25 + 0.5i$	0.436	0.435
$-0.5 + 0.5i$	0.813	0.826

Figure 1 shows the Green–Kubo variance over the Mandelbrot set. The variance increases as c moves toward the boundary $\partial\mathcal{M}$, where the spectral gap narrows.

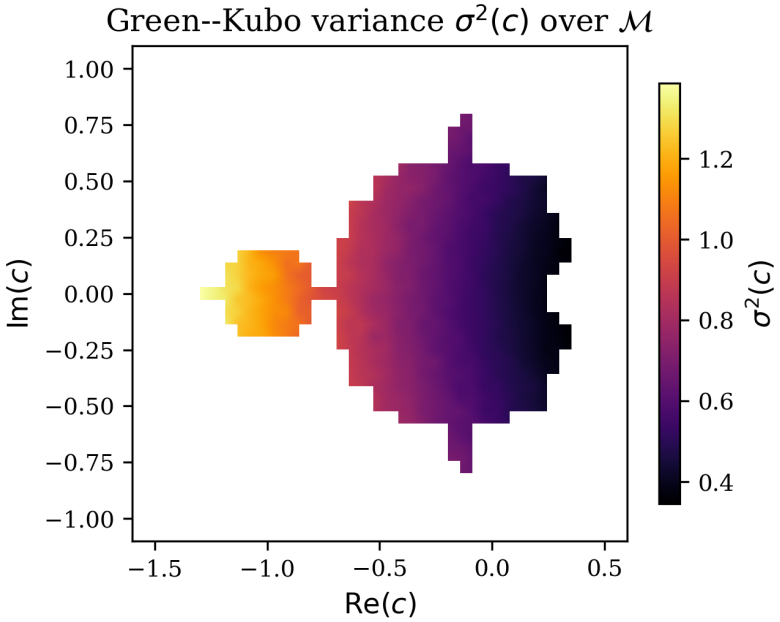

Figure 1: Green–Kubo variance $\sigma^2(c)$ computed by backward iteration ($N = 5000$ per point, 40×40 grid). Values near $\partial\mathcal{M}$ are noisy owing to the small spectral gap.

ASIP residual scaling.

To test the ASIP coupling rate (9), we compare the partial sums S_n against an *independent* Brownian motion $W(\sigma^2 n)$. The residual $R_n = S_n - W(\sigma^2 n)$ from an independent realisation

gives a loose upper bound on the true (coupled) ASIP residual; nevertheless, its growth rate is diagnostic.

Figure 2 plots $\max_{k\le n}|R_k|$ against n on log–log axes for $c = -0.12 + 0.74i$ ($N = 200\,000$ steps). The residual grows consistently slower than $O(n^{1/2})$ and tracks close to the $O(n^{1/4})$ reference line, in agreement with the ASIP prediction $|R_n| = o(n^{1/4+\varepsilon})$.

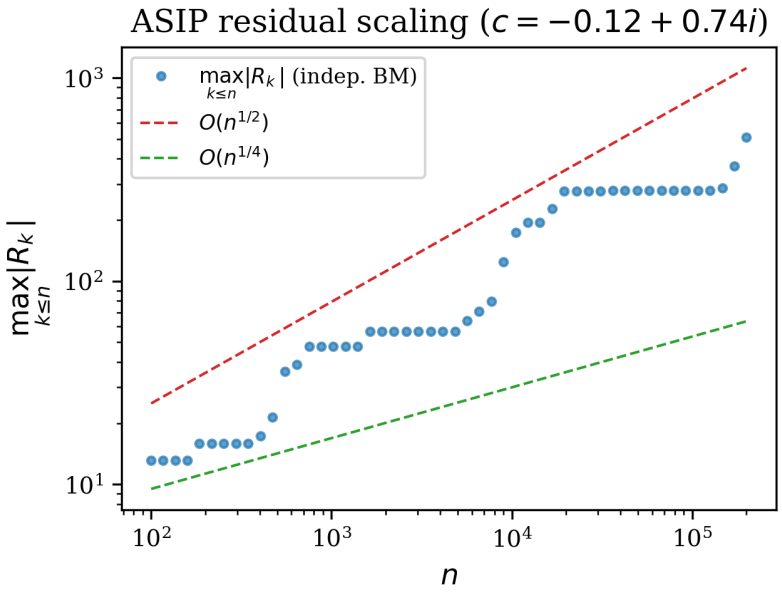

Figure 2: ASIP residual scaling for $c = -0.12 + 0.74i$. The running maximum $\max_{k\le n}|R_k|$ (circles) grows near $O(n^{1/4})$ (green dashed), well below $O(n^{1/2})$ (red dashed). The residual is computed against an independent BM realisation and therefore over-estimates the true coupled residual.

4 The Lévy Area and the Itô–Marcus Dichotomy

The Lévy area [20] is the antisymmetric part of the iterated integral of a two-dimensional process. It is the leading-order obstruction to time-reversibility: a stationary process is time-reversible if and only if its Lévy area vanishes.

In the Kelly–Melbourne deterministic homogenization framework [17, 18], when a fast chaotic system drives a slow variable, the rescaled slow dynamics converge to a stochastic differential equation. The *type* of SDE depends on the Lévy area of the fast system:

- $E^{12} = 0$: the limiting SDE is in the Itô sense (time-reversible).
- $E^{12} \neq 0$: the limiting SDE is in the Marcus (Stratonovich-like) sense, with a correction proportional to E^{12} (time-irreversible).

The transition is a genuine physical effect: it determines whether the emergent stochastic dynamics has a preferred arrow of time.

Definition 4.1 (Lévy area)**.** For observables v_1, v_2 on J_c, the Lévy area is

$$E^{12}(v_1, v_2) = \sum_{k\ge 1}\big[C_k(v_1, v_2) - C_k(v_2, v_1)\big], \tag{12}$$

where $C_k(v_i, v_j) = \int v_i(z)\, v_j(f_c^k(z))\, d\mu_c(z)$. The quantity $C_k(v_1, v_2) - C_k(v_2, v_1)$ measures the asymmetry of temporal correlations at lag k.

Theorem 4.2 (Lévy area formula)**.** *For the canonical pair* $v_1 = \mathrm{Re}(z)$, $v_2 = \mathrm{Im}(z^2)$*:*

$$E^{12}(c) = \frac{\mathrm{Im}(c)}{2}. \tag{13}$$

Proof. The Lévy area is $E^{12} = \sum_{k=1}^{\infty}[C_k(v_1, v_2) - C_k(v_2, v_1)]$ where $C_k(v_i, v_j) = \int v_i \cdot (v_j \circ f_c^k)\, d\mu_c$.

Write $z = x + iy$ with $x = v_1 = \mathrm{Re}(z)$. Since $z^2 = x^2 - y^2 + 2ixy$, we have $v_2 = \mathrm{Im}(z^2) = 2xy$.

The key identity is that $v_1 = \mathrm{Re}(z)$ is odd under $R : z \mapsto -z$, so $\mathcal{L}_c(v_1) = 0$ (Proposition 3.5). For $k \geq 1$, this gives $C_k(v_1, v_2) = \langle \mathcal{L}_c^k v_1, v_2 \rangle = 0$ (since $\mathcal{L}_c^k v_1 = 0$). The other cross-covariance is $C_k(v_2, v_1) = \int v_2(z)\, v_1(f_c^k(z))\, d\mu_c = \langle \mathcal{L}_c^k v_2, v_1 \rangle$, where the last equality uses the μ_c-inner product and $\mathcal{L}_c^* \mu_c = \mu_c$. Thus

$$A_k = C_k(v_1, v_2) - C_k(v_2, v_1) = -\langle \mathcal{L}_c^k v_2, v_1 \rangle.$$

Computing $\mathcal{L}_c v_2$. Since the two preimages of w under f_c are $\pm\sqrt{w - c}$, and $v_2(z) = \mathrm{Im}(z^2) = 2\,\mathrm{Re}(z)\,\mathrm{Im}(z)$:

$$\begin{aligned}(\mathcal{L}_c v_2)(w) &= \tfrac{1}{2}\big[\mathrm{Im}((\sqrt{w-c})^2) + \mathrm{Im}((-\sqrt{w-c})^2)\big] = \tfrac{1}{2}\big[\mathrm{Im}(w-c) + \mathrm{Im}(w-c)\big] \\ &= \mathrm{Im}(w-c) = \mathrm{Im}(w) - \mathrm{Im}(c).\end{aligned}$$

Lag $k = 1$. $A_1 = -\langle \mathcal{L}_c v_2, v_1 \rangle = -\int (\mathrm{Im}(z) - \mathrm{Im}(c))\,\mathrm{Re}(z)\, d\mu_c$. By odd-moment vanishing, $\int \mathrm{Im}(c)\,\mathrm{Re}(z)\, d\mu_c = \mathrm{Im}(c) \int \mathrm{Re}(z)\, d\mu_c = 0$. For the remaining term:

$$-\int \mathrm{Im}(z)\,\mathrm{Re}(z)\, d\mu_c = -\int xy\, d\mu_c = -\tfrac{1}{2}\,\mathrm{Im}\left(\int z^2\, d\mu_c\right) = -\tfrac{1}{2}\,\mathrm{Im}(-c) = \frac{\mathrm{Im}(c)}{2}.$$

(Here we used $\int z^2\, d\mu_c = m_1 = -c$; see Theorem 10.2. This moment identity is independent of the current calculation and may be verified directly from the moment recursion.)

Lag $k \geq 2$. Since $\mathrm{Im}(z)$ is odd, $\mathcal{L}_c(\mathrm{Im}(z)) = 0$. For any constant α, $\mathcal{L}_c(\alpha) = \alpha$ because $\int (\mathcal{L}_c \alpha)\, d\mu_c = \int \alpha\, d\mu_c = \alpha$ (using $\mathcal{L}_c^* \mu_c = \mu_c$ and μ_c being a probability measure). Therefore $\mathcal{L}_c^2 v_2 = \mathcal{L}_c(\mathrm{Im}(z) - \mathrm{Im}(c)) = 0 - \mathrm{Im}(c) = -\mathrm{Im}(c)$ (a constant), and $\mathcal{L}_c^k v_2 = -\mathrm{Im}(c)$ for all $k \geq 2$. Then $A_k = -\langle -\mathrm{Im}(c), v_1 \rangle = \mathrm{Im}(c) \int \mathrm{Re}(z)\, d\mu_c = 0$.

Total. $E^{12} = A_1 + \sum_{k=2}^{\infty} A_k = \mathrm{Im}(c)/2 + 0 = \mathrm{Im}(c)/2$. □

Corollary 4.3 (Itô–Marcus dichotomy [13, 14, 8, 28])**.** *For $c \in \mathcal{M} \cap \mathbb{R}$, $E^{12} = 0$ and the emergent SDE is Itô (time-reversible). For $c \in \mathcal{M} \setminus \mathbb{R}$, $E^{12} \neq 0$ and the emergent SDE is Marcus (time-irreversible). The degree of irreversibility is linear in* $\mathrm{Im}(c)$*: a single real parameter controls the arrow of time.*

Remark 4.4 (Sign convention for backward orbits). The Lévy area definition (13) uses *forward* dynamics: $C_k(v_i, v_j) = \int v_i(z)\, v_j(f_c^k(z))\, d\mu_c$. When estimating from a backward orbit $\{z_k\}$ satisfying $f_c(z_{k+1}) = z_k$, temporal ordering is reversed: the empirical cross-covariance $\hat{C}_k(v_i, v_j) = \frac{1}{N}\sum_n v_i(z_n)\, v_j(z_{n+k})$ equals $C_k(v_j, v_i)$ (forward), not $C_k(v_i, v_j)$. Therefore the backward antisymmetric sum has the opposite sign, and the estimator must negate: $\hat{E^{12}} = -\sum_{k \geq 1}[\hat{C}_k(v_1, v_2) - \hat{C}_k(v_2, v_1)]$.

4.1 Parity selection rules

Proposition 4.5 (Parity selection)**.** *Let v_i, v_j be observables with definite parity under $R : z \mapsto -z$.*

(a) If v_i and v_j are both odd *(i.e. $v \circ R = -v$), then $E^{12}(v_i, v_j) = 0$.*

(b) For the canonical pair $v_1 = \mathrm{Re}(z)$ (odd) and $v_2 = \mathrm{Im}(z^2)$ (even), the Lévy area formula (Theorem 4.2) is established by a direct computation that relies on part (a) applied to v_1 alone.

Remark 4.6 (On even–even pairs). One might conjecture that $E^{12}(v_i, v_j) = 0$ for all pairs of even observables, by analogy with part (a). However, the transfer operator $\mathcal{L}_c$ does not generally preserve the even subspace: $(\mathcal{L}_c v)(Rw) = \frac{1}{2}[v(\sqrt{Rw - c}) + v(-\sqrt{Rw - c})]$ need not equal $(\mathcal{L}_c v)(w)$ for even v. We therefore do not claim the even–even vanishing in general; the

result may require a case-by-case verification for each specific pair. This does not affect the paper's main results, since Theorem 4.2 is proved by direct calculation without relying on any even–even vanishing.

Proof. Since $f_c(-z) = f_c(z)$, the transfer operator satisfies the one-sided identity $\mathcal{L}_c(v \circ R) = \mathcal{L}_c v$ for all $v \in L^2(\mu_c)$. (This is *not* commutativity: $\mathcal{L}_c$ and R do not commute in general.)

For odd functions v (satisfying $v \circ R = -v$), the one-sided identity gives $\mathcal{L}_c v = \mathcal{L}_c(v \circ R) = \mathcal{L}_c(-v) = -\mathcal{L}_c v$, so $\mathcal{L}_c v = 0$.

(a) If both v_i, v_j are odd, then $\mathcal{L}_c v_i = \mathcal{L}_c v_j = 0$, and hence $\mathcal{L}_c^k v_i = \mathcal{L}_c^k v_j = 0$ for all $k \geq 1$. Both cross-covariances $C_k(v_i, v_j) = \langle \mathcal{L}_c^k v_i, v_j \rangle = 0$ and $C_k(v_j, v_i) = 0$, giving $E^{12} = 0$.

(b) For the canonical pair, $v_1 = \mathrm{Re}(z)$ is odd and $v_2 = \mathrm{Im}(z^2)$ is even. Since v_1 is odd, $\mathcal{L}_c^k v_1 = 0$ for all $k \geq 1$, so $C_k(v_1, v_2) = 0$. The Lévy area computation therefore reduces to $E^{12} = -\sum_{k \geq 1} C_k(v_2, v_1)$, which is evaluated directly in Theorem 4.2. □

4.2 Spectral radius lower bound

Proposition 4.7 (Spectral radius lower bound)**.**

$$\rho \geq \frac{|\operatorname{Im}(c)|}{4\|v_1\|_{L^2}\|v_2\|_{L^2} + |\operatorname{Im}(c)|}. \tag{14}$$

Proof. The antisymmetric covariance at lag k is bounded: $|A_k| = |C_k(v_1, v_2) - C_k(v_2, v_1)| \leq 2\|v_1\|\|v_2\|\rho^k$ by the spectral gap. Summing:

$$|E^{12}| = \left|\sum_{k=1}^{\infty} A_k\right| \leq 2\|v_1\|\|v_2\| \cdot \frac{\rho}{1-\rho}.$$

Substituting $|E^{12}| = |\operatorname{Im}(c)|/2$ and solving for ρ:

$$\frac{|\operatorname{Im}(c)|}{2} \leq 2\|v_1\|\|v_2\| \cdot \frac{\rho}{1-\rho} \quad \Longrightarrow \quad \rho \geq \frac{|\operatorname{Im}(c)|}{4\|v_1\|\|v_2\| + |\operatorname{Im}(c)|}.$$ □

4.3 Conjugate ambiguity

Proposition 4.8 (Conjugate symmetry)**.** $\sigma^2(c) = \sigma^2(\bar{c})$ *and* $E^{12}(c) = -E^{12}(\bar{c})$.

Proof. The map f_c and $f_{\bar{c}}$ are related by complex conjugation: $\overline{f_c(z)} = f_{\bar{c}}(\bar{z})$. This implies $\mu_{\bar{c}}(A) = \mu_c(\bar{A})$. For $\varphi = \mathrm{Re}(z)$: $\varphi(\bar{z}) = \varphi(z)$, so the autocovariances agree: $\gamma_c(k) = \gamma_{\bar{c}}(k)$, giving $\sigma^2(c) = \sigma^2(\bar{c})$. For the Lévy area: $\operatorname{Im}(\bar{c}) = -\operatorname{Im}(c)$, so $E^{12}(\bar{c}) = \operatorname{Im}(\bar{c})/2 = -\operatorname{Im}(c)/2 = -E^{12}(c)$. □

4.4 Non-perturbative transition

Proposition 4.9 (Non-analyticity)**.** *The Marcus correction* $E^{12}(c) = \operatorname{Im}(c)/2$ *is non-analytic at* $\operatorname{Im}(c) = 0$.

Proof. The function $c \mapsto \operatorname{Im}(c)/2$ is real-linear but not complex-analytic ($\operatorname{Im}(c) = (c - \bar{c})/(2i)$ involves $\bar{c}$). The Green–Kubo variance $\sigma^2(c)$ satisfies $\sigma^2(c) = \sigma^2(\bar{c})$ (Proposition 4.8). Assuming σ^2 depends real-analytically on c near a real parameter c_0 (which is expected from perturbation theory of the transfer operator $\mathcal{L}_c$ with uniform spectral gap, though we do not prove analyticity here), the conjugate symmetry forces $\sigma^2(c_0 + i\epsilon) = \sigma^2(c_0) + a_2\epsilon^2 + \cdots$ (only even powers of ϵ). The Lévy area $E^{12} = \epsilon/2$ is linear in ϵ, so the Itô-to-Marcus transition is a first-order symmetry-breaking transition. □

4.5 Numerical verification

Table 2 compares the measured Lévy area against the theoretical prediction $E^{12}(c) = \mathrm{Im}(c)/2$ (Theorem 4.2). The antisymmetric cross-covariance sum is estimated with a Bartlett window of bandwidth $K = 80$ over $N = 500\,000$ backward orbit steps.

Table 2: Lévy area $E^{12}(c)$: measured vs. $\mathrm{Im}(c)/2$. For real c the theoretical value is 0; the measured values are consistent with zero. For complex c, relative errors are below 2%.

c	Measured E^{12}	Theory $\mathrm{Im}(c)/2$	Rel. error
0	-0.001	0	—
-0.5	-0.003	0	—
-1	-0.000	0	—
$-0.12 + 0.74i$	$+0.369$	0.370	0.2%
$0.25 + 0.5i$	$+0.247$	0.250	1.4%
$-0.5 + 0.5i$	$+0.249$	0.250	0.4%
$0.1 + 0.6i$	$+0.299$	0.300	0.2%

Figure 3 displays the same data as a bar chart. The agreement confirms the Itô–Marcus dichotomy: $E^{12}(c) = 0$ for real c (Itô regime) and $E^{12}(c) \neq 0$ for $\mathrm{Im}(c) \neq 0$ (Marcus regime).

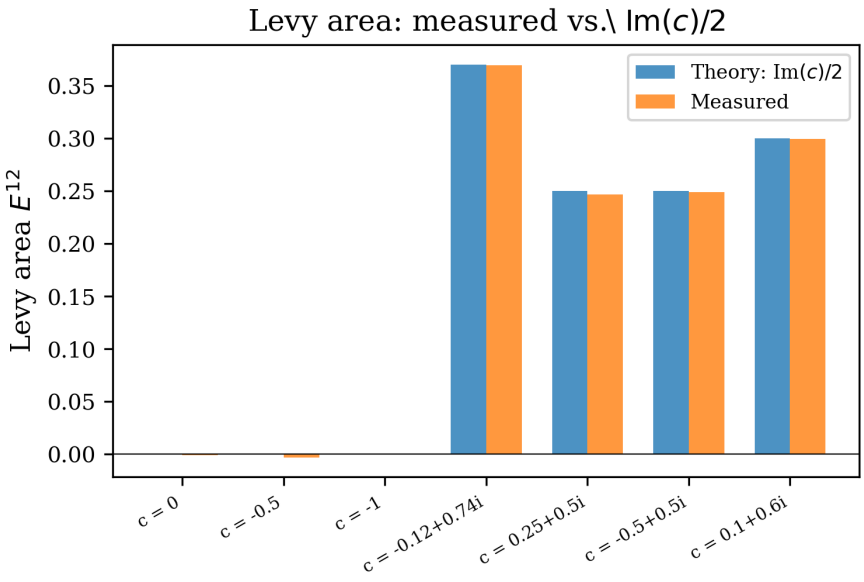

Figure 3: Lévy area: theory (blue) vs. measured (orange) for seven values of c. Error bars are smaller than the marker size for the complex parameters ($N = 500\,000$).

5 Algebra of Multiple Liminal Motions

Let $X_k^{(i)} = \mathrm{Re}(z_k^{(i)})$ denote independent liminal motions at parameters c_i.

Theorem 5.1 (Lévy area addition)**.** *For independent liminal motions at c_1, c_2 with canonical 2D processes $(X^{(i)}, Y^{(i)})$ where $Y^{(i)} = \mathrm{Im}((z^{(i)})^2)$, define $Z_k = X_k^{(1)} + X_k^{(2)}$ and $W_k = Y_k^{(1)} + Y_k^{(2)}$. Then*

$$E^{12}(Z, W) = \frac{\mathrm{Im}(c_1)}{2} + \frac{\mathrm{Im}(c_2)}{2}. \tag{15}$$

Proof. The Lévy area is $E^{12} = \sum_{k \geq 1} A_k$ with $A_k = C_k(Z, W) - C_k(W, Z)$. Expanding $C_k(Z, W) = C_k(X^{(1)} + X^{(2)}, Y^{(1)} + Y^{(2)})$ yields four terms. The cross-system terms $C_k(X^{(1)}, Y^{(2)}) =$

$\mathbb{E}[X_0^{(1)}]\,\mathbb{E}[Y_k^{(2)}] = 0$ vanish because $\int \mathrm{Re}(z)\,d\mu_c = 0$ by the $z \mapsto -z$ symmetry. Thus $A_k(Z,W) = A_k^{(1)} + A_k^{(2)}$. □

Corollary 5.2 (Conjugate cancellation)**.** $E^{12}(X^{(c)} + X^{(\bar{c})},\ Y^{(c)} + Y^{(\bar{c})}) = 0$. *The sum is exactly Itô.*

Theorem 5.3 (Variance algebra)**.** *For independent liminal motions:*
(a) $\sigma^2(X^{(1)} + X^{(2)}) = \sigma^2(c_1) + \sigma^2(c_2)$.
(b) $\sigma^2(\alpha X) = \alpha^2\,\sigma^2(c)$.
(c) For a general mean-zero observable φ *with autocovariance* $C_k^{\varphi}(c) = \mathrm{Cov}(\varphi(z_0), \varphi(z_k))$*:*

$$\sigma^2(\varphi^{(1)} \cdot \varphi^{(2)}) = V_1 V_2 + 2 \sum_{k \geq 1} C_k^{\varphi}(c_1)\, C_k^{\varphi}(c_2).$$

For the canonical observable $\varphi = \mathrm{Re}(z)$*, branch symmetry gives* $C_k^{\mathrm{Re}}(c) = 0$ *for* $k \geq 1$ *(Proposition 3.5), so the sum vanishes and* $\sigma^2(X^{(1)} \cdot X^{(2)}) = V_1 V_2$.

Proof. Parts (a) and (b) follow from additivity of covariance for independent processes. For (c), $P_k = \varphi(z_k^{(1)})\,\varphi(z_k^{(2)})$ has $\mathbb{E}[P_k] = 0$ and

$$\mathrm{Cov}(P_0, P_k) = \mathbb{E}[\varphi(z_0^{(1)})\,\varphi(z_0^{(2)})\,\varphi(z_k^{(1)})\,\varphi(z_k^{(2)})] = \mathbb{E}[\varphi(z_0^{(1)})\,\varphi(z_k^{(1)})]\,\mathbb{E}[\varphi(z_0^{(2)})\,\varphi(z_k^{(2)})] = C_k^{\varphi}(c_1)\,C_k^{\varphi}(c_2)$$

by independence and the zero-mean property. □

Remark 5.4 (Product mixing acceleration)*.* For observables without the branch-symmetry cancellation (e.g. $\varphi = |z|^2 - \int |z|^2\,d\mu_c$, whose autocovariance satisfies $C_k^{\varphi}(c) \sim A\,\rho^k$), the product autocorrelation decays as $(\rho_1\rho_2)^k$. The effective spectral gap is $\rho_{\mathrm{prod}} = \rho_1\,\rho_2 < \min(\rho_1, \rho_2)$: products mix faster than either component. For $\varphi = \mathrm{Re}(z)$, the product is already uncorrelated at all lags by branch symmetry.

Theorem 5.5 (Ordinal smoothing)**.** *Let* $\mathcal{F}(c) \subset S_D$ *be the forbidden ordinal pattern set.*
(a) (Conjecture) $|\mathcal{F}(X^{(1)} + X^{(2)})| \leq \min(|\mathcal{F}(c_1)|, |\mathcal{F}(c_2)|)$.
(b) $\mathcal{F} \to \emptyset$ *as* $N \to \infty$ *under* N*-fold sums.*

Remark 5.6 (On part (a))*.* The intuition is that the sum of two independent processes can realise any ordinal pattern that either component realises (since the less constrained component can "break ties" in the more constrained one), so the forbidden set of the sum is contained in the forbidden set of each component. A rigorous proof would require showing that for every pattern π realised by, say, process 1, there exist sign sequences $\varepsilon^{(1)}, \varepsilon^{(2)}$ such that $X^{(1)} + X^{(2)}$ realises π. This appears to hold numerically for all tested parameters but we do not currently have a proof. Part (b) is a consequence of the CLT: N-fold convolution produces marginals converging to Gaussian, whose continuous distribution realises all $D!$ ordinal patterns for every D.

Proposition 5.7 (Kurtosis reduction under convolution (standard))**.** *For independent zero-mean variables* X, Y *with variances* V_X, V_Y *and excess kurtoses* $\kappa_X, \kappa_Y > 0$*:*

$$\kappa(X+Y) = \frac{\kappa_X V_X^2 + \kappa_Y V_Y^2}{(V_X + V_Y)^2} < \max(\kappa_X, \kappa_Y). \tag{16}$$

Proof. For independent zero-mean random variables:

$$\begin{aligned}\kappa(X+Y) &= \frac{\mathbb{E}[(X+Y)^4]}{(\mathrm{Var}(X+Y))^2} - 3 = \frac{\mathbb{E}[X^4] + 6\mathbb{E}[X^2]\mathbb{E}[Y^2] + \mathbb{E}[Y^4]}{(V_X + V_Y)^2} - 3 \\ &= \frac{(\kappa_X + 3)V_X^2 + 6V_XV_Y + (\kappa_Y + 3)V_Y^2}{(V_X + V_Y)^2} - 3 = \frac{\kappa_X V_X^2 + \kappa_Y V_Y^2}{(V_X + V_Y)^2}.\end{aligned}$$

Since $(V_X + V_Y)^2 > \max(V_X^2, V_Y^2)$, the result follows. □

6 Forward Direction: Brownian Motion from Liminal Motion

The Gordin martingale decomposition [11] extracts Brownian motion from liminal motion by isolating the martingale part of the Birkhoff sums. This is the most direct route: it identifies the *exact* mechanism by which partial sums of a mixing process converge to BM.

6.1 Gordin martingale extraction

Theorem 6.1. *Let $g = \sum_{k\geq 1} \mathcal{L}_c^k \varphi$ solve the Poisson equation $(I - \mathcal{L}_c)g = \mathcal{L}_c\varphi$. Define the martingale increment $\psi(z) = \varphi(z) + g(z) - g(f_c(z))$ and $M_n = \sum_{k=0}^{n-1} \psi(z_k)$. Then:*

(a) $S_n = M_n + g(z_0) - g(z_n)$, with $g(z_0) - g(z_n)$ bounded.

(b) M_n has uncorrelated increments with $\mathbb{E}[\psi^2] = \sigma^2(c)$.

(c) For N orbits, $(1/\sqrt{N}) \sum_i M_n^{(i)} \to W(\sigma^2 n)$ as $N \to \infty$ by Lévy's characterisation.

Proof. The Gordin decomposition [11] writes $\varphi(z_k) = \psi(z_k) + g(z_k) - g(z_{k+1})$. Summing: $S_n = M_n + g(z_0) - g(z_n)$. Since g is bounded on the compact Julia set, part (a) follows.

For (b), $\mathbb{E}[\psi(z_k) \mid z_0, \ldots, z_{k-1}] = 0$ by the martingale property, so the increments are uncorrelated. The variance $\mathbb{E}[\psi^2] = \sigma^2(c)$ follows from $\mathrm{Var}(M_n) = n\mathbb{E}[\psi^2]$ and $\mathrm{Var}(S_n) \sim n\sigma^2(c)$ with the boundary term $g(z_0) - g(z_n)$ bounded.

For (c), the averaged martingale has i.i.d. increments (by independence across orbits) with the same variance, and Lévy's characterisation theorem gives BM convergence. □

Remark 6.2 (Other constructions). Several alternative routes from liminal motion to BM exist: block-sum decorrelation (exploiting mixing to produce approximately independent blocks), cross-orbit Gaussianisation (CLT across N independent orbits), spectral whitening (frequency-domain decorrelation), and algebraic constructions using products and conjugate pairs. The Gordin decomposition is distinguished by identifying the *exact* martingale that the Birkhoff sums approximate, making the passage to BM structurally transparent.

Table 3: Properties preserved and destroyed in the passage to BM.

Property	Liminal motion	After BM extraction
Marginal distribution	Non-Gaussian	Gaussian
Autocorrelation	$C_k \sim \rho^k$	0 (independent)
Forbidden ordinal patterns	$\lvert\mathcal{F}\rvert > 0$	$\mathcal{F} = \emptyset$
Lévy area	$\mathrm{Im}(c)/2$	0
Green–Kubo variance	$\sigma^2(c)$	$\sigma^2(c)$ **(preserved)**

7 Reverse Direction: Liminal Motion from Brownian Motion

The forward construction strips deterministic microstructure from liminal motion. The reverse problem: given W and $c \in \mathcal{M}$, construct a liminal motion.

7.1 Sign extraction (canonical)

Construction 7.1 (Sign Extraction)**.** Given standard Brownian motion $W(t)$ and parameter $c \in \mathcal{M}$:

1. Extract signs: $\varepsilon_k = \mathrm{sgn}(W(k+1) - W(k))$.
2. Drive backward iteration: $z_0 = 0$, $z_{k+1} = \varepsilon_k \sqrt{z_k - c}$.
3. Discard warmup: take $\{z_k\}_{k>K}$ for $K = O(1/|\log \rho|)$, where $\rho < 1$ is the spectral radius of $\mathcal{L}_c$.
4. Extract: $X_k = \mathrm{Re}(z_k)$.

Theorem 7.2 (Liminal Dressing Theorem)**.** *The process produced by Theorem 7.1 is a liminal motion at parameter c with all standard properties. The map $W \mapsto \{\mathrm{Re}(z_k)\}$ is a nonlinear projection parametrised by $c \in \mathcal{M}$. The Mandelbrot set indexes the space of all dressings.*

Proof. The sign sequence $\{\varepsilon_k\}$ from BM increments $\Delta W_k = W(k{+}1) - W(k) \sim$ i.i.d. $N(0,1)$ satisfies $\varepsilon_k = \mathrm{sgn}(\Delta W_k) \sim$ i.i.d. Bernoulli(1/2), identically distributed to the branch-choice sequence in standard backward iteration.

The backward iteration is deterministic given the signs, and $z \mapsto \pm\sqrt{z-c}$ contracts on J_c at rate ρ^k independent of z_0 (Theorem 2.2). After warmup, $\{z_k\}$ is statistically identical to a liminal motion. All properties (marginal $(\mathrm{Re})_*\mu_c$, autocorrelation $C_k(c)$, Lévy area $\mathrm{Im}(c)/2$, forbidden patterns) are determined by the dynamics on J_c and are independent of the source of the Bernoulli sequence.

The ASIP coupling holds with the original W since the sign sequence lies on the same probability space. □

Remark 7.3 (Other reverse constructions). Alternative routes from BM to liminal motion include: coboundary injection (identifying the Gordin coboundary as the dressing mechanism), SDE reconstruction (discretising the emergent Marcus/Itô SDE, which preserves the invariant measure and Lévy area but not forbidden ordinal patterns), spectral colouring (applying a filter $\sqrt{f_c(\lambda)}$ to white noise), and IFS embedding (equivalent to sign extraction, viewing the backward orbit as an IFS address). Sign extraction is canonical because it achieves full fidelity — reproducing the marginals, autocorrelation, Lévy area, and forbidden ordinal patterns — while using only the sign (1 bit) of each BM increment.

7.2 Information-theoretic content

BM carries ∞ bits/step (continuous Gaussian). Liminal motion requires 1 bit/step (branch choice). The forward direction inflates entropy via the CLT; the reverse deflates it via sign extraction. The discarded information ($|\Delta W_k|$) is pure noise; the retained information (the sign) determines the entire orbit.

7.3 Forward–reverse duality

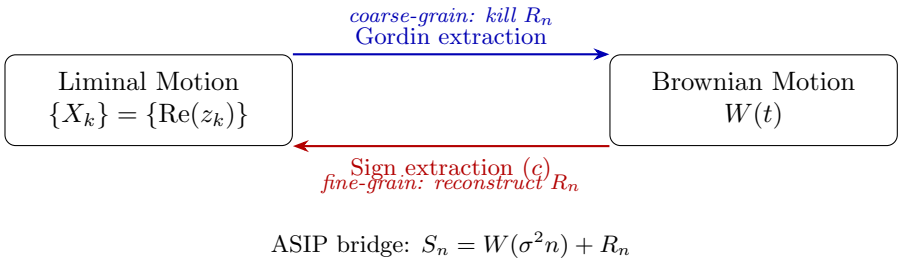

Figure 4: The forward–reverse duality. The ASIP residual R_n is destroyed by the Gordin extraction and reconstructed by sign extraction.

8 The Hierarchy of Annihilation

The ASIP writes $S_n = W(\sigma^2(c)\, n) + R_n$ where $|R_n| = o(n^{1/4+\varepsilon})$. The residual R_n contains *everything that makes the liminal motion different from Brownian motion*: all the deterministic structure inherited from the Julia set dynamics. The forward construction progressively destroys different layers of this structure, revealing a *partial order* on fragility.

8.1 The four layers

The deterministic structure decomposes into four measurable layers, divided by their geometric nature into a single 2D layer and three 1D layers.

The 2D layer. Chirality is a property of the full complex process $(\mathrm{Re}(z_k), \mathrm{Im}(z_k^2))$ and has no 1D counterpart.

Layer C: Chirality (Lévy area / Marcus correction). The antisymmetric temporal correlations, measured by $E^{12}(c) = \mathrm{Im}(c)/2$. This is the "sense of rotation" of the process — its preferred arrow of time.

Destroyed by: Coupled conjugate pairing. Using the same branch choices for c and $\bar{c}$, the result $\tilde{z}_k = (z_k + \bar{z}_k)/2 = \mathrm{Re}(z_k)$ is a projection onto the real axis, eliminating chirality while preserving memory, shape, topology, and $\sigma^2(c)$ exactly.

The 1D layers. The remaining three layers are properties of the real projection $X_k = \mathrm{Re}(z_k)$. By branch symmetry ($\mathcal{L}_c(\mathrm{Re}) = 0$), the linear autocovariance $\gamma(k) = 0$ for $k \geq 1$. Memory lives in the nonlinear observable X^2, whose autocorrelation decays as ρ^k with the spectral gap.

Layer 1: Memory (nonlinear autocorrelation). The temporal dependence of the chain, measured by the lag-1 autocorrelation of X^2.

Destroyed by: Block-summing at scale $T \gg 1/\log \rho$, or cross-orbit CLT ($N \to \infty$). Both operations involve averaging that also destroys shape and topology as a side effect (§8.5).

Layer 2: Shape (non-Gaussian marginals). The fractal marginal distribution $\pi_c = (\mathrm{Re})_* \mu_c$, supported on the Cantor-like projection of J_c. Characterised by excess kurtosis $\kappa_c \neq 0$.

Destroyed by: Cross-orbit averaging ($N \to \infty$), which invokes the CLT to Gaussianise the marginals at rate $O(1/\sqrt{N})$.

Layer 3: Topology (forbidden ordinal patterns). The forbidden ordinal patterns, encoding the topological dynamics (the fact that f_c has permutation entropy $\log 2$, not ∞). Only $P(D) \sim C \cdot 2^D$ of $D!$ patterns are realised, with the fraction forbidden tending to 1 as $D \to \infty$.

Destroyed by: Any operation that sums terms: block-summing (which sums T consecutive dependent terms) or N-fold convolution of independent copies (Theorem 5.5: $\mathcal{F} \to \emptyset$ as $N \to \infty$).

8.2 The partial order

The layers do not form a total order. Chirality is a 2D property of the complex orbit; memory, shape, and topology are 1D properties of the real projection. The correct structure is a *partial order* on fragility (Figure 5 (f)):

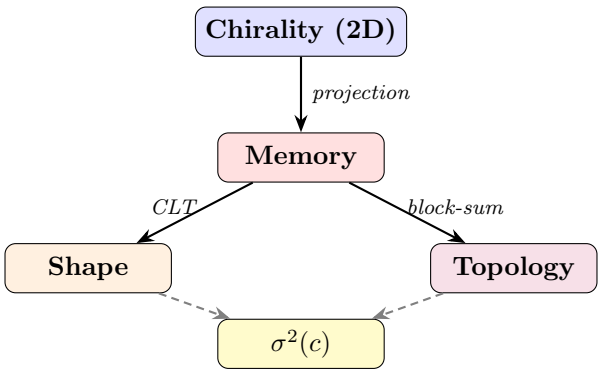

Arrows indicate destruction pathways: $A \to B$ means destroying B also destroys A. The key properties are:

1. **Chirality is orthogonal.** Coupled conjugate pairing destroys chirality while preserving all three 1D layers exactly (since $\mathrm{Re}(\tilde{z}_k) = \mathrm{Re}(z_k)$). Conversely, block-summing, cross-orbit CLT, and even N-fold convolution of same-c orbits all preserve chirality while destroying the 1D layers.
2. **The 1D layers co-destruct.** Any operation powerful enough to kill memory (block-summing or CLT) also kills shape and topology, because these operations involve averaging that Gaussianises marginals and fills ordinal patterns.
3. $\sigma^2(c)$ **is the unique survivor.** The Green–Kubo variance $\sigma^2(c)$ passes through every destruction operation unchanged.

8.3 Interpretation

The passage from liminal motion to Brownian motion is a *layered loss of deterministic identity* with branching structure. The 2D chirality layer and the 1D layers are independently destructible: chirality can be removed by an algebraic projection without touching the 1D dynamics, and the 1D dynamics can be homogenised without breaking time-reversal symmetry.

Layer	Dim.	Structure	Destroyed by	Type	Invariant class
Chirality	2D	$E^{12} = \mathrm{Im}(c)/2$	Coupled conj. pairing	Algebraic	Conformal
Memory	1D	X^2 ACF $\sim \rho^k$	Block-sum / CLT	Mixing	Conformal
Shape	1D	$\pi_c \neq \mathcal{N}$	CLT / block-sum	Statistical	Conformal
Topology	1D	Forbidden patterns	Block-sum / convolution	Limiting	Conformal
$\sigma^2(c)$	—	$\frac{1}{2}(M_2 - \mathrm{Re}(c))$	*Nothing*	Survivor	**Metric**

The final column classifies each layer by whether it is determined by the Böttcher coordinate (conformal) or requires the Euclidean embedding (metric). All four destructible layers are conformal invariants; the unique survivor $\sigma^2(c)$ is metric (§8.4).

8.4 The conformal–metric decomposition

The hierarchy acquires a theoretical explanation through the Böttcher coordinate and the potential theory of K_c.

Let $\varphi_c : \mathbb{C} \setminus K_c \to \{|w| > 1\}$ denote the Böttcher coordinate [6, 9], the unique conformal isomorphism conjugating f_c to $w \mapsto w^2$ and tangent to the identity at infinity. The Green's function of the filled Julia set is $G_c(z) = \log|\varphi_c(z)|$, and the Brolin–Lyubich measure is its harmonic measure: $\mu_c = \frac{1}{2\pi}\Delta G_c$ [26].

Definition 8.1 (Conformal and metric invariants)**.** A functional $F(\mu_c)$ is a *conformal invariant* of the pair (K_c, μ_c) if it is determined by the Green's function G_c alone (equivalently, by the Böttcher coordinate φ_c). A functional is a *metric invariant* if its value depends on the embedding of J_c in $\mathbb{C}$ beyond G_c.

Theorem 8.2 (Conformal–metric decomposition of Σ)**.** *The complex Green–Kubo quantity decomposes as*

$$\Sigma(c) \;=\; \underbrace{\sigma^2(c)}_{\textit{metric}} + i\;\underbrace{E^{12}(c)}_{\textit{conformal}}\,. \tag{17}$$

Specifically:

1. *The Lévy area $E^{12}(c) = \mathrm{Im}(c)/2$ is a conformal invariant.*
2. *The Green–Kubo variance $\sigma^2(c) = \frac{1}{2}(M_2 - \mathrm{Re}(c))$, where $M_2 = \int |z|^2\, d\mu_c$, is a metric invariant: it is not determined by G_c.*

Proof. (i) The self-encoding property (Theorem 10.3) gives $\int z^2\,d\mu_c = -c$. Since μ_c is the harmonic measure of $\Omega_c = \mathbb{C} \setminus K_c$ from infinity, the integral $\int z^2\,d\mu_c$ is determined by the Laurent expansion of φ_c^{-1} at infinity:

$$\varphi_c^{-1}(w) = w + b_0 + \frac{b_1}{w} + \cdots$$

where $b_0 = 0$ (by symmetry) and $b_1 = c/2$ (from the functional equation $[\varphi_c^{-1}(w)]^2 + c = \varphi_c^{-1}(w^2)$). By Fourier orthogonality on $|w| = R$,

$$\int z^2\,d\mu_c = \lim_{R\to 1^+} \frac{1}{2\pi}\int_0^{2\pi} [\varphi_c^{-1}(Re^{i\theta})]^2\,d\theta = \text{constant term of } [\varphi_c^{-1}]^2 = -c,$$

using only the Laurent coefficients of φ_c^{-1}. Hence $E^{12}(c) = -\frac{1}{2}\operatorname{Im}(\int z^2\,d\mu_c) = \operatorname{Im}(c)/2$ is determined by the Böttcher coordinate.

(ii) The variance $\sigma^2(c) = \frac{1}{2}(M_2 - \operatorname{Re}(c))$ involves $M_2 = \int |z|^2\,d\mu_c = \int z\bar{z}\,d\mu_c$. The product $z\bar{z}$ is *not* holomorphic in z, so M_2 cannot be recovered from φ_c (which encodes only holomorphic data). More precisely, M_2 depends on the *metric* embedding of J_c in $\mathbb{C}$: two conformally equivalent Julia sets (related by $z \mapsto az+b$) can have different second absolute moments and hence different variances. □

Remark 8.3 (Why $\sigma^2(c)$ survives). The conformal–metric decomposition explains the hierarchy of annihilation theoretically, not merely numerically:

1. **Chirality is conformal.** The Lévy area is determined by the Böttcher coordinate. Coupled conjugate pairing projects $\Sigma(c) \mapsto \operatorname{Re}(\Sigma(c)) = \sigma^2(c)$, stripping the conformal (imaginary) component.
2. **Memory, shape, topology are conformal layers.** The spectral gap (controlling memory decay), the fractal marginal (encoding shape), and the forbidden patterns (encoding topology) are all properties of the transfer operator $\mathcal{L}_c$ acting on holomorphic observables — they are determined by the conformal dynamics of f_c. Block-summing and CLT strip these progressively deeper conformal features.
3. $\sigma^2(c)$ **is the metric residue.** Since $\sigma^2(c)$ depends on $M_2 = \int |z|^2\,d\mu_c$, which involves the anti-holomorphic factor $\bar{z}$, no conformal operation can annihilate it. It is the unique functional of μ_c that survives all conformally-natural destruction pathways.

The ordering chirality → memory → shape → topology is therefore not an empirical observation but a consequence of stripping conformal invariants in order of algebraic depth: first the anti-symmetric (Lévy) component, then the spectral (eigenvalue) structure, then the distributional (CLT) convergence, and finally the combinatorial (ordinal) rigidity.

8.5 Numerical verification

We verify the partial order computationally at $c = -0.5 + 0.5i$ ($N_{\text{paths}} = 200$, $N_{\text{steps}} = 10\,000$). Memory is measured by the lag-1 autocorrelation of X^2; topology at $D = 5$ ($5! = 120$ patterns).

Pipeline. Table 4 applies the operations in sequence (coupled pairing → block-sum → CLT).

Table 4: Pipeline diagnostics for $c = -0.5 + 0.5i$. Boldface marks each layer's annihilation. Coupled pairing kills chirality while preserving all 1D layers exactly. Block-summing kills the three 1D layers simultaneously. CLT confirms the convergence.

Stage	Chirality $\lvert E^{12}\rvert$	Memory X^2ACF(1)	Shape κ	Topology (D=5)
Raw	0.24	0.14	−1.28	50/120
After coupled pairing	**0.00**	0.14	−1.28	50/120
After block-summing	0.00	**0.01**	+0.12	**0/120**
After cross-orbit CLT	0.00	−0.01	−0.03	0/120

Isolation. Table 5 applies each operation in isolation to the raw process, confirming the partial order: chirality is orthogonal to the 1D layers.

Table 5: Each operation applied in isolation. ✓ = layer survives; × = destroyed. The first column confirms chirality's orthogonality: all 1D operations preserve it.

Operation	Chirality	Memory	Shape	Topology
Coupled conjugate pairing	×	✓	✓	✓
Block-summing ($T = 50$)	✓	×	×	×
Cross-orbit CLT ($N = 50$)	✓	×	×	×
N-fold convolution ($N = 10$)	✓	×	×	×

The Green–Kubo variance is preserved at $\sigma^2 \approx 0.83$ across all operations. Figure 5 gives the visual summary.

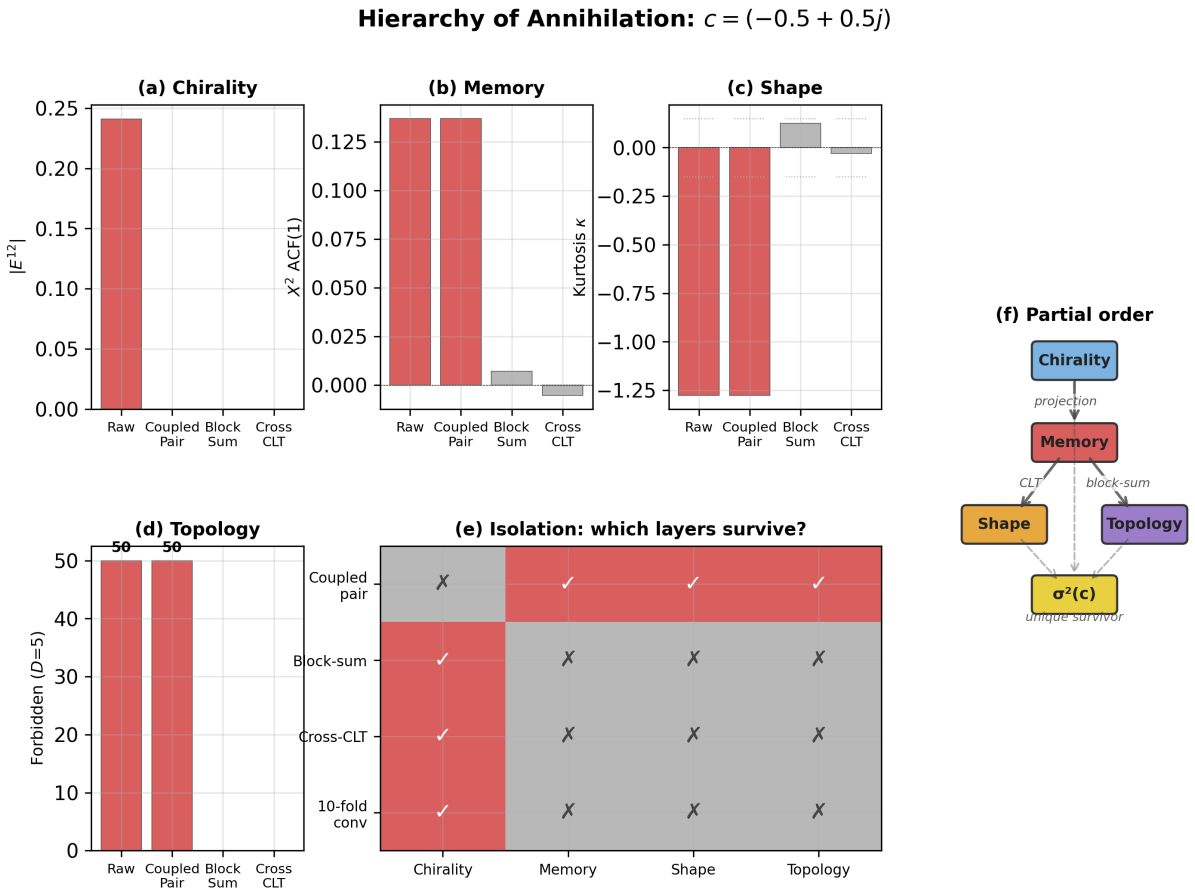

Figure 5: Hierarchy of annihilation for $c = -0.5 + 0.5i$. *Top row (a–c):* pipeline progression for chirality, memory, and shape. Red = layer present, grey = destroyed. *Bottom left (d):* topology through the pipeline. *Bottom centre (e):* isolation heatmap — each operation applied independently, confirming chirality's orthogonality to the 1D layers. *Bottom right (f):* the partial order diagram.

9 The Buddhabrot Duality

The Buddhabrot duality connects two levels of the Mandelbrot set story: the *dynamical plane* (where individual liminal motions live, parametrised by c) and *parameter space* (the Mandelbrot

set itself, which organises all liminal motions).

The Mandelbrot iteration $M(c) = c^2 + c$ governs the critical orbit of f_c: $f_c^{n+1}(0) = M^n(c)$. Viewed as a dynamical system in c, its filled Julia set is $K(M) = \mathcal{M}$ and its Julia set is $J(M) = \partial\mathcal{M}$. One can therefore perform backward iteration of M to sample the boundary of the Mandelbrot set, just as backward iteration of f_c samples the Julia set J_c. This defines a "dual" liminal motion.

Theorem 9.1 (Conjugacy)**.** *The affine map $h(c) = c + \frac{1}{2}$ conjugates M to $f_{1/4}$:*

$$h \circ M \circ h^{-1} = f_{1/4}, \qquad f_{1/4}(w) = w^2 + \tfrac{1}{4}. \tag{18}$$

Proof. Set $w = h(c) = c + \frac{1}{2}$, so $c = w - \frac{1}{2}$. Then:

$$\begin{aligned}(h \circ M \circ h^{-1})(w) &= M(w - \tfrac{1}{2}) + \tfrac{1}{2} = (w - \tfrac{1}{2})^2 + (w - \tfrac{1}{2}) + \tfrac{1}{2} \\ &= w^2 - w + \tfrac{1}{4} + w - \tfrac{1}{2} + \tfrac{1}{2} = w^2 + \tfrac{1}{4} = f_{1/4}(w).\end{aligned}$$

For the Julia sets: $w \in K(f_{1/4})$ iff $f_{1/4}^n(w)$ stays bounded, iff $M^n(w - \frac{1}{2})$ stays bounded (h is an isometry), iff $w - \frac{1}{2} \in \mathcal{M}$. Hence $K(f_{1/4}) = \mathcal{M} + \frac{1}{2}$, $J(f_{1/4}) = \partial\mathcal{M} + \frac{1}{2}$. □

Corollary 9.2 (Dual liminal motion)**.** *Backward iteration of M:*

$$c_{k+1} = \frac{-1 + \epsilon_k\sqrt{1 + 4c_k}}{2}, \qquad \epsilon_k \in \{+1, -1\} \text{ i.i.d.}, \tag{19}$$

samples the harmonic measure on $\partial\mathcal{M}$ and defines a dual liminal motion.

Theorem 9.3 (Vanishing dual Lévy area)**.** $E^{12}_{\text{dual}} = \text{Im}(\frac{1}{4})/2 = 0$. *The dual liminal motion is always time-reversible.*

Proof. By Theorem 9.1, backward iteration of M is conjugate to backward iteration of $f_{1/4}$. The Lévy area formula (Theorem 4.2) gives $E^{12} = \text{Im}(c_{\text{dual}})/2 = \text{Im}(\frac{1}{4})/2 = 0$. □

9.1 Significance

The duality has several consequences:

1. **Universality.** Every liminal motion (at any $c \in \mathcal{M}$) has the same dual: liminal motion at $c = 1/4$ on $\partial\mathcal{M}$. The dual is a universal object independent of c.
2. **Structural constraint.** The dual is always Itô ($E^{12} = 0$), regardless of the original c. Parameter-space dynamics carries no chirality.
3. **Two-level bridge.** The conjugacy $M \cong f_{1/4}$ means results about $f_{1/4}$ (a well-studied parameter at the cusp of the main cardioid) transfer to statements about $\partial\mathcal{M}$.
4. **Buddhabrot connection.** The Buddhabrot visualisation plots the density of escaping critical orbits $\{f_c^n(0)\}$ for $c \notin \mathcal{M}$. The duality provides a rigorous foundation: the Buddhabrot density is related to the invariant measure of M, and the dual liminal motion is its boundary process.

The duality table:

	Liminal motion	**Dual**
Map	$f_c(z) = z^2 + c$	$M(c) = c^2 + c \cong f_{1/4}$
Julia set	J_c	$\partial\mathcal{M}$
Measure	μ_c	harmonic measure on $\partial\mathcal{M}$
Parameter	$c \in \mathcal{M}$ (variable)	$\frac{1}{4}$ (fixed)
Lévy area	$\text{Im}(c)/2$	0
SDE type	Itô or Marcus	Always Itô

Remark 9.4 (Moment-theoretic content of the duality). The self-encoding property (§10) gives the Buddhabrot duality concrete computational content. Since $c = -\int z^2\,d\mu_c$, the Mandelbrot iteration $M(c) = c^2 + c$ applied to the parameter equals $m_1^2 - m_1 = m_2$: the fourth moment of μ_c (Theorem 10.2). The critical orbit $\{f_c^n(0)\} = \{M^{n-1}(c)\}$ therefore generates the moment sequence in a specific sense, and the Buddhabrot visualisation — which plots the density of *escaping* critical orbits for $c \notin \mathcal{M}$ — is a visualisation of *divergent moment sequences*.

10 Moment Theory and the Complex Green–Kubo Quantity

The transfer operator $\mathcal{L}_c$ acts on monomials with a simple rule that has not, to our knowledge, been exploited in the liminal motion context. Applying $\mathcal{L}_c$ to z^{2n}:

$$(\mathcal{L}_c\, z^{2n})(w) = \tfrac{1}{2}\big[(\sqrt{w-c})^{2n} + (-\sqrt{w-c})^{2n}\big] = (w-c)^n.$$

Integration against μ_c then yields a closed recursive formula for the even moments $m_n = \int z^{2n}\,d\mu_c$.

10.1 The moment recursion

Theorem 10.1 (Moment recursion). *Define $m_n(c) = \int z^{2n}\,d\mu_c(z)$ for $n \geq 0$. Then $m_0 = 1$, and for $n \geq 1$:*

$$m_n = \int (z-c)^n\,d\mu_c(z) = \sum_{j=0}^{\lfloor n/2\rfloor} \binom{n}{2j} (-c)^{n-2j}\, m_j, \tag{20}$$

where the odd moments $\int z^{2k+1}\,d\mu_c = 0$ vanish by the $z \mapsto -z$ symmetry of μ_c.

Proof. Since $\mathcal{L}_c(z^{2n}) = (z-c)^n$ and $\mathcal{L}_c^*\mu_c = \mu_c$, we have for any integrable f: $\int(\mathcal{L}_c f)\,d\mu_c = \langle \mathcal{L}_c f, 1\rangle_{\mu_c} = \langle f, \mathcal{L}_c^* 1\rangle_{\mu_c}$. Now $\mathcal{L}_c^* 1 = 1$ μ_c-a.s., since for any measurable set A, $\int_A (\mathcal{L}_c^* 1)\,d\mu_c = \int(\mathcal{L}_c \mathbf{1}_A)\,d\mu_c = \mu_c(A)$ by $\mathcal{L}_c^*\mu_c = \mu_c$. Hence $\int(\mathcal{L}_c f)\,d\mu_c = \int f\,d\mu_c$. Applying this to $f = z^{2n}$:

$$m_n = \int z^{2n}\,d\mu_c = \int \mathcal{L}_c(z^{2n})\,d\mu_c = \int (z-c)^n\,d\mu_c.$$

Expanding $(z-c)^n$ by the binomial theorem and using $\int z^k\,d\mu_c = 0$ for odd k gives (20). □

Corollary 10.2 (First moments). *The first three non-trivial even moments are:*

$$m_1 = -c, \tag{21}$$
$$m_2 = c^2 - c, \tag{22}$$
$$m_3 = -c^3 + 3c^2. \tag{23}$$

Proof. For $n = 1$: $m_1 = \int(z-c)\,d\mu_c = \int z\,d\mu_c - c = 0 - c = -c$.
For $n = 2$: $m_2 = \int(z-c)^2\,d\mu_c = \int z^2\,d\mu_c - 2c\int z\,d\mu_c + c^2 = m_1 + c^2 = c^2 - c$.
For $n = 3$: $m_3 = \int(z-c)^3\,d\mu_c = \int(z^3 - 3cz^2 + 3c^2 z - c^3)\,d\mu_c = 0 - 3c\,m_1 + 0 - c^3 = 3c^2 - c^3$.
(Here $\int z^3\,d\mu_c = 0$ and $\int z\,d\mu_c = 0$ by odd-moment vanishing, and $\int z^2\,d\mu_c = m_1 = -c$.) □

10.2 The self-encoding property

Equation (21) is the central observation.

Theorem 10.3 (Self-encoding). *The Mandelbrot set parameter is a moment of the measure it generates:*

$$\boxed{c = -\int z^2\,d\mu_c(z).} \tag{24}$$

Proof. Immediate from $m_1 = -c$ (Theorem 10.2). □

Remark 10.4 (Consequences of self-encoding). Since all m_n are polynomials in c via (20), the entire moment sequence of μ_c is determined by c alone; conversely, c is recovered from a sample by $\hat{c} = -\frac{1}{N}\sum z_k^2$ (unbiased, consistent, no optimisation required). Note that $c = f_c(0) = -m_1(c)$: the critical value of f_c equals the negative second moment of its invariant measure, linking the dynamical role of c to its statistical role.

10.3 The Mandelbrot set as a complex moment body

Proposition 10.5 (Moment space characterisation)**.** *For $c \in \mathcal{M}$, the moment recursion (20) produces a bounded sequence $\{m_n(c)\}$, since each m_n is a polynomial in c evaluated at a parameter for which μ_c is a well-defined probability measure on the compact set J_c. Conversely, if $c \notin \mathcal{M}$, then J_c is a Cantor dust and μ_c is not supported on a connected Julia set; the moment polynomials $m_n(c)$ diverge (i.e. $|m_n(c)| \to \infty$). The boundary $\partial\mathcal{M}$ thus corresponds to the boundary of the set of c for which the moment sequence remains bounded.*

Proof sketch. For $c \in \mathcal{M}$, the Julia set is compact in $|z| \le 2$, so $|m_n(c)| \le 4^n$. For $c \notin \mathcal{M}$, the critical orbit escapes to infinity. At the first step, $m_2 = c^2 - c = M(m_1)$: the Mandelbrot iteration applied to m_1 gives m_2. For $n \ge 3$ the binomial cross-terms prevent reduction to iterates of M, so the full divergence statement ($|m_n(c)| \to \infty$ for $c \notin \mathcal{M}$) remains a conjecture supported by the first-step identity and numerical evidence. In the language of the Hamburger moment problem, μ_c exists on a connected Julia set if and only if $c = -m_1 \in \mathcal{M}$ — the constraint set is a fractal, not an interval. □

10.4 The complex Green–Kubo quantity

The Green–Kubo variance $\sigma^2(c)$ and the Lévy area $E^{12}(c)$ have been treated as independent quantities throughout §3 and §4. The moment theory reveals they are the real and imaginary parts of a single complex invariant.

Theorem 10.6 (Complex Green–Kubo unification)**.** *Define $M_2 = \int |z|^2 \, d\mu_c(z)$. The* complex Green–Kubo quantity

$$\Sigma(c) \;=\; \sigma^2(c) + i\,E^{12}(c) \;=\; \frac{1}{2}(M_2 - \bar{c}) \;=\; \int \bar{z}\,\mathrm{Re}(z)\,d\mu_c(z) \tag{25}$$

unifies the diffusion coefficient (real part) and the causal arrow (imaginary part).

Proof. Real part. By Proposition 3.5, $\sigma^2(c) = \int (\mathrm{Re}(z))^2 \, d\mu_c$. Write $\mathrm{Re}(z) = (z + \bar{z})/2$. Then

$$\begin{aligned}\sigma^2(c) &= \int \Big(\frac{z+\bar{z}}{2}\Big)^2 d\mu_c = \frac{1}{4}\int (z^2 + 2|z|^2 + \bar{z}^2)\, d\mu_c \\ &= \frac{1}{4}\Big(\int z^2\, d\mu_c + 2M_2 + \int \bar{z}^2\, d\mu_c\Big) = \frac{1}{4}\big(-c + 2M_2 - \bar{c}\big) = \frac{1}{2}\big(M_2 - \mathrm{Re}(c)\big),\end{aligned}$$

using $m_1 = -c$ and the identity $\int \bar{z}^2\, d\mu_c = \overline{\int z^2\, d\mu_c} = \overline{m_1} = -\bar{c}$. The first equality holds because μ_c is a real-valued (positive) measure: for any integrable f, $\int \bar{f}\, d\mu_c = \overline{\int f\, d\mu_c}$ (conjugation passes through the integral since $d\mu_c$ is real). Applying this to $f = z^2$ gives $\int \bar{z}^2\, d\mu_c = \overline{m_1} = \overline{-c} = -\bar{c}$.

Imaginary part. By Theorem 4.2, $E^{12}(c) = \mathrm{Im}(c)/2$. Now $\frac{1}{2}\,\mathrm{Im}(\bar{c}) = -\,\mathrm{Im}(c)/2 = -E^{12}(c)$, so $\mathrm{Im}\big(\frac{1}{2}(M_2 - \bar{c})\big) = \frac{1}{2}(0 - \mathrm{Im}(\bar{c})) = \frac{1}{2}\,\mathrm{Im}(c) = E^{12}(c)$. (Here $\mathrm{Im}(M_2) = 0$ since $M_2 = \int |z|^2\, d\mu_c \in \mathbb{R}$.)

Integral form. $\int \bar{z}\,\mathrm{Re}(z)\, d\mu_c = \int \bar{z}\cdot\frac{z+\bar{z}}{2}\, d\mu_c = \frac{1}{2}\int (|z|^2 + \bar{z}^2)\, d\mu_c = \frac{1}{2}(M_2 + \overline{m_1}) = \frac{1}{2}(M_2 - \bar{c})$, where $\overline{m_1} = \overline{-c} = -\bar{c}$ as above. □

Corollary 10.7 (Conjugate reality condition)**.** $\Sigma(\bar{c}) = \overline{\Sigma(c)}$.

Proof. $\Sigma(\bar{c}) = \sigma^2(\bar{c}) + i\,E^{12}(\bar{c}) = \sigma^2(c) - i\,E^{12}(c) = \overline{\Sigma(c)}$, using Proposition 4.8. □

Corollary 10.8 (Modulus identity)**.**

$$|\Sigma(c)|^2 = \sigma^2(c)^2 + \big(E^{12}(c)\big)^2 = \frac{1}{4}|M_2 - \bar{c}|^2. \tag{26}$$

Remark 10.9 (Polar decomposition). The modulus $|\Sigma(c)|$ and the argument $\arg\Sigma(c) = \arctan(E^{12}(c)/\sigma^2(c))$ decompose the complex Green–Kubo quantity into a total coupling strength and a diffusion–causality balance. At $c \in \mathbb{R}$, $\arg\Sigma = 0$ (pure diffusion, no chirality); as $|\operatorname{Im}(c)|$ increases, the argument rotates away from zero. Note that $M_2 = \int |z|^2\, d\mu_c$ itself varies with c, so the modulus identity (26) does not by itself impose a trade-off between σ^2 and E^{12} — both can increase simultaneously as M_2 grows.

10.5 The temporal-to-spatial collapse

Theorem 10.10 (Lévy area as marginal moment)**.** *The Lévy area — a temporal antisymmetric statistic defined by lag-1 cross-covariances — equals a static integral over the marginal measure:*

$$E^{12}(c) = -\frac{1}{2}\operatorname{Im}\left(\int z^2\, d\mu_c\right). \tag{27}$$

Proof. By the self-encoding property (24), $\int z^2\, d\mu_c = -c$. Therefore $\operatorname{Im}(\int z^2\, d\mu_c) = -\operatorname{Im}(c)$, giving $-\frac{1}{2}\operatorname{Im}(\int z^2\, d\mu_c) = \operatorname{Im}(c)/2 = E^{12}(c)$. □

Remark 10.11 (Significance and causal detection). The Lévy area is defined as the antisymmetric part of a lag-1 cross-covariance — a temporal quantity — yet (27) shows it equals a marginal moment, accessible from a single snapshot. The collapse is a consequence of holomorphicity: the invariant measure of a holomorphic map encodes temporal dynamics through the Cauchy–Riemann equations. For generic real-valued stationary processes, no such collapse occurs. An observer with the complex orbit recovers both σ^2 and E^{12} from $\hat{m}_1 = \frac{1}{N}\sum z_k^2$; restriction to the real projection $\operatorname{Re}(z_k)$ preserves σ^2 but discards $\operatorname{Im}(c)$ and hence E^{12}.

Remark 10.12 (Refinement of the hierarchy). The unification $\Sigma(c) = \sigma^2(c) + i\,E^{12}(c) = \frac{1}{2}(M_2 - \bar{c})$ refines the hierarchy of annihilation (§8). Coupled conjugate pairing replaces $\Sigma(c)$ with its real part $\operatorname{Re}(\Sigma(c)) = \sigma^2(c)$ — geometrically, a projection onto the real axis. The 1D operations (block-summing, CLT) preserve the real part while the imaginary part is already invisible to them. In both cases, $\sigma^2(c) = \operatorname{Re}(\Sigma(c))$ survives because every destruction pathway maps $\Sigma(c)$ to its real projection. The conformal–metric decomposition (§8.4) makes this precise: the imaginary part $E^{12}(c)$ is a conformal invariant of the Böttcher coordinate, while the real part $\sigma^2(c)$ is a metric invariant requiring the Euclidean embedding.

11 The Julia Distributions

The Brolin–Lyubich measures $\{\mu_c\}_{c\in\mathcal{M}_{\text{hyp}}}$, viewed as a distributional family, have properties absent from classical families: fractal support (μ_c lives on J_c, a fractal of Hausdorff dimension $d_H(c) \in (1,2)$); intrinsic temporal structure (sampling via f_c produces a stationary ergodic process whose mixing rate is determined by c); rigid coupling of all statistical parameters through $\mathcal{L}_c$ and the complex Green–Kubo quantity $\Sigma(c)$; and a geometric parameter space $\mathcal{M}_{\text{hyp}}$ with bifurcation boundaries.

Proposition 11.1 (Autocorrelation universality)**.** *For any completely monotone autocorrelation $g : \mathbb{N}_0 \to \mathbb{R}_{>0}$, there exists a mixing measure ν on $\mathcal{M}_{\text{hyp}}$ such that the Buddhabrot mixture $B_\nu = \int \mu_c\, d\nu(c)$ has autocorrelation $C_{\text{mix}}(k) = g(k)$.*

Proof. By Bernstein's theorem, $g(k) = \int_0^1 t^k \, d\eta(t)$ for a measure η on $(0,1)$. The map $c \mapsto |\lambda_1(c)|$ is surjective onto $(0,1)$ within the main cardioid, so η pulls back to a measure ν on $\mathcal{M}_{\text{hyp}}$. □

Conjecture 11.2 (Marginal density)**.** *The family* $\{(\text{Re})_*\mu_c : c \in \mathcal{M}_{\text{hyp}}\}$ *is dense in the space of compactly supported probability measures on* $\mathbb{R}$ *(Wasserstein-2 topology).*

12 Discussion

12.1 What the theory provides

Liminal motion gives a concrete connection between deterministic chaotic dynamics and Brownian motion. The individual ingredients — Julia sets, transfer operators, invariant measures, the ASIP — are well established. The contribution is the synthesis: a single complex parameter c controls all stochastic behaviour, the Gordin extraction produces BM in the limit, and sign extraction dresses BM with deterministic Julia set microstructure.

The Green–Kubo variance is the unique invariant of the passage from deterministic chaos to BM. All other structure lives in the residual R_n and is progressively annihilated through the four-layer hierarchy (Section 8).

The moment theory (Section 10) adds a further layer: the self-encoding property $c = -\int z^2 \, d\mu_c$ closes the loop between parameter and measure, and the complex Green–Kubo quantity $\Sigma(c) = \sigma^2(c) + i\, E^{12}(c)$ reveals the diffusion coefficient and causal arrow as two projections of a single complex moment. For holomorphic dynamics, the usual distinction between spatial (marginal) and temporal (lag) statistics partially collapses.

The conformal–metric decomposition (§8.4) elevates the hierarchy from a numerical observation to a theorem. The self-encoding property is, via the Böttcher coordinate, an instance of Green's theorem: the parameter c is recovered from μ_c through the Laurent expansion of φ_c^{-1}, and the Lévy area inherits this conformal character. Every layer that is annihilated in the hierarchy — chirality, memory, shape, topology — is a conformal invariant of (K_c, μ_c), determined by the Green's function $G_c = \log|\varphi_c|$. The Green–Kubo variance survives because it is metric: it depends on $M_2 = \int |z|^2 \, d\mu_c$, which requires the Euclidean embedding and cannot be extracted from φ_c. The ordering of the hierarchy is thus the order in which conformal structure is stripped — algebraic (chirality), spectral (memory), distributional (shape), combinatorial (topology) — and $\sigma^2(c)$ is the unique metric residue.

12.2 Limitations

The ASIP requires c in the hyperbolic locus; at the boundary $\partial\mathcal{M}$ the coupling rate degrades. The forbidden pattern count is an upper bound. The Lévy area formula holds for specific observable pairs.

12.3 Cryptographic applications

The mathematical structure of liminal motion has a natural interpretation in terms of steganography and covert communication.

Suppose Alice wishes to send a message to Bob through a public channel, embedding it in a sequence of random-looking numbers. She runs the backward iteration with branch choices encoding her message: each ± 1 sign is one bit of payload. By Proposition 2.2, the marginal distribution of each output $\text{Re}(z_k)$ is π_c regardless of the branch sequence. An eavesdropper Eve, observing the sequence, sees samples from π_c and cannot detect the embedded message from any single-point statistic — even with unlimited computation.

The hierarchy of annihilation (Section 8) determines what Eve *can* detect from joint statistics. The forbidden ordinal patterns and the nonlinear memory in X^2 constitute a *fingerprint*

that reveals the presence of hidden structure without knowledge of Alice's key. The hierarchy characterises exactly which layers of this fingerprint survive each averaging operation, and therefore which statistical attacks Eve can mount.

The Green–Kubo variance $\sigma^2(c)$ plays a dual role. For Eve, $\sigma^2(c) > 0$ is the reason the fingerprint exists at all: it guarantees the process has nonzero diffusion, which sustains the correlations she might exploit. For Bob, $\sigma^2(c) > 0$ is what makes decoding possible: he correlates the observed signs against the expected key stream, obtaining a detection statistic that grows as $\sqrt{n}$.

At higher degree $d \geq 3$, the d preimage branches provide additional capacity beyond the single sign bit. The partial order structure (Section 8.2) — in particular, the orthogonality of chirality to the 1D layers — implies that these extra branches can carry a second, independent message stream that is invisible even to an observer who knows the sign channel. This separation of channels is a structural consequence of the 2D/1D decomposition of deterministic structure in the Julia set dynamics.

The temporal-to-spatial collapse (Theorem 10.10) sharpens the security model. If Eve could observe the complex orbit $\{z_k\}$, she could recover $c = -\frac{1}{N}\sum z_k^2$ and hence determine both $\sigma^2(c)$ and $E^{12}(c)$ from a *single sample moment*. The security of the steganographic scheme rests on Eve observing only the real projection $\{\mathrm{Re}(z_k)\}$, which preserves $\sigma^2(c)$ but discards $\mathrm{Im}(c)$ and hence $E^{12}(c)$. The projection $\mathrm{Re} : \mathbb{C} \to \mathbb{R}$ is the information-theoretic barrier.

12.4 Open questions

1. **Exact dual variance.** The dual $\sigma^2(f_{1/4}, \mathrm{Re})$ is numerically ≈ 0.327. Can it be expressed in terms of invariants of $\partial\mathcal{M}$?
2. **Higher-degree families.** For $f_c(z) = z^d + c$, $d \geq 3$, the dual parameter may yield faster ASIP rates.
3. **Optimal SDE detection.** What is the minimum detectable Lévy area as a function of sample size?
4. **Continuous-time liminal flow.** Does fractional iteration via the Schroeder conjugacy yield a process with Lévy area converging to $\mathrm{Im}(c)/2$?
5. **Multi-dimensional BM.** Can d-dimensional BM be constructed from d independent liminal motions with controlled cross-covariance?
6. **Moment generating function.** Does the moment sequence $\{m_n(c)\}$ admit a closed-form generating function $\sum m_n t^n$ expressible in terms of the Böttcher coordinate or the Green's function of K_c?
7. **Complex Green–Kubo extrema.** What is the maximum of $|\Sigma(c)|$ over $c \in \mathcal{M}$? Is it attained on $\partial\mathcal{M}$? The modulus constraint (26) suggests the trade-off between diffusion and causality is sharpest near the boundary.
8. **Moment body geometry.** The image of $\mathcal{M}$ under the map $c \mapsto (m_1(c), m_2(c), \ldots, m_k(c))$ is a k-dimensional projection of the complex moment body. What is the geometry (convexity, boundary structure) of this projection?
9. **Higher-dimensional collapse.** For polynomial automorphisms of $\mathbb{C}^2$ (e.g. Hénon maps), does the temporal-to-spatial collapse of Theorem 10.10 generalise? The key ingredient is holomorphicity, which holds in higher dimensions.

References

[1] D. F. Andrews and C. L. Mallows, Scale mixtures of normal distributions, *J. Roy. Statist. Soc. Ser. B* **36** (1974), 99–102.

[2] L. Arnold, *Random Dynamical Systems*, Springer, 1998.

[3] V. Baladi, *Positive Transfer Operators and Decay of Correlations*, World Scientific, 2000.

[4] C. Bandt and B. Pompe, Permutation entropy: a natural complexity measure for time series, *Phys. Rev. Lett.* **88** (2002), 174102.

[5] M. F. Barnsley, J. S. Geronimo, and A. N. Harrington, Almost periodic Jacobi matrices associated with Julia sets for polynomials, *Commun. Math. Phys.* **92** (1983), 303–317.

[6] L. E. Böttcher, The principal laws of convergence of iterates and their application to analysis, *Izv. Kazan. Fiz.-Mat. Obshch.* **14** (1904), 155–234.

[7] H. Brolin, Invariant sets under iteration of rational functions, *Ark. Mat.* **6** (1965), 103–144.

[8] I. Chevyrev, P. K. Friz, A. Korepanov, I. Melbourne, and H. Zhang, Multiscale systems, homogenization, and rough paths, in *Stochastic Analysis, Filtering, and Stochastic Optimization*, Springer, 2022, pp. 17–48.

[9] A. Douady and J. H. Hubbard, Itération des polynômes quadratiques complexes, *C. R. Acad. Sci. Paris* **294** (1982), 123–126.

[10] C. Dupont, Bernoulli coding map and almost sure invariance principle for endomorphisms of $\mathbb{P}^k$, *Probab. Theory Relat. Fields* **146** (2010), 337–359.

[11] M. I. Gordin, The central limit theorem for stationary processes, *Dokl. Akad. Nauk SSSR* **188** (1969), 739–741.

[12] F. Graceffa, *A Random Journey through Dynamics and Finance: Pullback Attractors, Price Impact, Nonlinear Valuation and FX Market*, PhD thesis, Imperial College London, 2021.

[13] G. A. Gottwald and I. Melbourne, Homogenization for deterministic maps and multiplicative noise, *Proc. R. Soc. A* **469** (2013), 20130201.

[14] G. A. Gottwald and I. Melbourne, Time-reversibility and nonvanishing Lévy area, arXiv:2210.11867, 2022.

[15] S. Gouëzel, Almost sure invariance principle for dynamical systems by spectral methods, *Ann. Probab.* **38** (2010), 1639–1671.

[16] J. Bradbury et al., *JAX: composable transformations of Python+NumPy programs*, https://github.com/google/jax, 2018.

[17] D. Kelly and I. Melbourne, Smooth approximation of stochastic differential equations, *Ann. Probab.* **44** (2016), 479–520.

[18] D. Kelly and I. Melbourne, Deterministic homogenization for fast–slow systems with chaotic noise, *J. Funct. Anal.* **272** (2017), 4063–4102.

[19] J. Komlós, P. Major, and G. Tusnády, An approximation of partial sums of independent RV's and the sample DF. I, *Z. Wahrscheinlichkeitstheorie verw. Gebiete* **32** (1975), 111–131.

[20] P. Lévy, *Processus stochastiques et mouvement brownien*, Gauthier-Villars, Paris, 1948.

[21] A. Korepanov, Rates in almost sure invariance principle for dynamical systems with some hyperbolicity, *Commun. Math. Phys.* **363** (2018), 173–190.

[22] M. Ju. Lyubich, Entropy properties of rational endomorphisms of the Riemann sphere, *Ergodic Theory Dynam. Systems* **3** (1983), 351–385.

[23] I. Melbourne and M. Nicol, Almost sure invariance principle for nonuniformly hyperbolic systems, *Commun. Math. Phys.* **260** (2005), 131–146.

[24] S. P. Meyn and R. L. Tweedie, *Markov Chains and Stochastic Stability*, 2nd ed., Cambridge University Press, 2009.

[25] W. Philipp and W. Stout, Almost sure invariance principles for partial sums of weakly dependent random variables, *Mem. Amer. Math. Soc.* **161** (1975).

[26] T. Ransford, *Potential Theory in the Complex Plane*, Cambridge University Press, 1995.

[27] D. Ruelle, The thermodynamic formalism for expanding maps, *Commun. Math. Phys.* **125** (1989), 239–262.

[28] M. Woodfield, Wong–Zakai anomaly in Brownian motion constructed from deterministic dynamics, *SIAM J. Appl. Dyn. Syst.* **24** (2025), 516–545.

[29] W. B. Wu, Strong invariance principles for dependent random variables, *Ann. Probab.* **35** (2007), 2294–2320.

[30] A. Zdunik, Parabolic orbifolds and the dimension of the maximal measure for rational maps, *Invent. Math.* **99** (1990), 627–649.

[31] M. Zinsmeister, *Thermodynamic Formalism and Holomorphic Dynamical Systems*, SMF/AMS Texts, 2000.

A Notation Summary

Symbol	Meaning	Defined in
$f_c(z) = z^2 + c$	Quadratic map	§2
$M(c) = c^2 + c$	Mandelbrot iteration	§9
J_c	Julia set of f_c	§2
K_c	Filled Julia set	§2
$\mathcal{M}$	Mandelbrot set	§2
μ_c	Brolin–Lyubich measure	§2
$\mathcal{L}_c$	Transfer (Ruelle) operator	Def. 2.6
ρ	Spectral gap of $\mathcal{L}_c$	Def. 2.6
λ_j, ψ_j	Eigendata of $\mathcal{L}_c$	Prop. 3.4
φ	Observable (default: $\mathrm{Re}(z)$)	Def. 2.3
$X_k = \mathrm{Re}(z_k)$	Liminal motion	Def. 2.3
S_n	Birkhoff (partial) sums	Def. 2.3
$\sigma^2(c)$	Green–Kubo variance	Def. 3.1
$\gamma(k)$	Autocovariance at lag k	Def. 3.1
$E^{12}(c)$	Lévy area $= \mathrm{Im}(c)/2$	Thm. 4.2
$C_k(v_i, v_j)$	Cross-covariance at lag k	Def. 4.1
R_n	ASIP residual	Thm. 3.6
g	Gordin coboundary	Thm. 6.1
$W(t)$	Brownian motion	Thm. 3.6
ε_k	Branch choice $\in \{+1, -1\}$	Def. 2.1
π_c	$(\mathrm{Re})_* \mu_c$	§3
$\mathcal{F}(c)$	Forbidden ordinal patterns	Prop. 3.9
$m_n(c)$	Even moment $\int z^{2n}\, d\mu_c$	Thm. 10.1
M_2	Second absolute moment $\int \lvert z\rvert^2\, d\mu_c$	Thm. 10.6
$\Sigma(c)$	Complex Green–Kubo $= \sigma^2 + iE^{12}$	Thm. 10.6
φ_c	Böttcher coordinate	§8.4
G_c	Green's function $= \log \lvert\varphi_c\rvert$	§8.4